An Intercomparison of 2-D Models Within a Common Framework

Debra K. Weisenstein, Malcolm K. W. Ko, Courtney J. Scott, Charles H. Jackman, Eric L. Fleming, David B. Considine, Douglas E. Kinnison, Peter S. Connell, and Douglas A. Rotman

Brief, Popular Summary of the Paper:

Atmospheric computer models have been used for about the last 30 years to help researchers understand the response of stratospheric ozone to various natural and human-made variations. Two-dimensional (latitude versus altitude) models have been developed in this time period and include a representation of transport and most of the chemical processes important in driving global ozone changes. Both the atmospheric transport and chemistry are important in the computation of ozone levels, thus calculated ozone variations from human-induced changes are dependent on both the transport and chemistry representation in the individual model.

The three two-dimensional (2-D) models AER, LLNL, and GSFC were developed at Atmospheric and Environmental Research in Cambridge, MA, Lawrence Livermore National Laboratory in Livermore, CA, and Goddard Space Flight Center in Greenbelt, MD, respectively. These models have been used extensively since the mid-1980's to assess the influence of various human-made impacts on stratospheric ozone.

Until this study it has been difficult to understand the differences in results from these three models since each model was developed separately by different groups of investigators and were dependent on both the transport and chemistry representation. The AER team was able to develop a common framework a few years ago that included the most relevant parts of the LLNL and GSFC models. With this common framework the three models could be compared much more quantitatively and the transport and chemistry portions of each model could be separated and compared individually with one another.

Differences in the model simulations of long-lived gases pointed out the transport differences among the models and the variations in the simulations of families of more reactive gases pointed out the chemistry differences. Simulations of the influence of the proposed High Speed Civil Transport (HSCT) planes indicated huge transport and cold polar process driven differences among the models.

JOURNAL OF GI OPHYSICAL RESEARCH, VOL. , NO. , PAGES 1 31,

An Intercomparison of 2-D Models Within a Common Framework

Debra K. Weisenstein, Malcolm K.W. Ko, and Courtney J. Scott

Atmospheric and Environmental Research, Lexington, Massachusetts

Charles H. Jackman, Eric L. Fleming[1], and David B. Considine[2]

NASA Goddard Space Flight Center, Greenbelt, Maryland

Douglas E. Kinnison[3], Peter S. Connell, and Douglas A. Rotman

Lawrence Livermore National Laboratory, Livermore, California

To appear in the *Journal of Geophysical Research*, 2001.

M. K. W. Ko, C. J. Scot , and D. K. Weisenstein, Atmospheric and Environmental Research, Inc., 131 Hartwell Ave , Lexington, MA 02421. (e-mail: mkwko@aer.com; scott@aer.com; dkweis@aer.com)

D. B. Considine, E. L. Fleming, and C. H. Jackman, NASA Goddard Space Flight Center, Greenbelt, MD 20771. (e-mail: dbc@welkin.larc.nasa.gov; fleming@kahuna.gsfc.nasa.gov; jackman@assess.gsfc.nasa.gov)

P. S. Connell, D. E. Kinnison, and D. A. Rotman Lawrence Livermore National Laboratory, Livermore, CA 94550. (e-mai : connell2@llnl.gov; dkin@ucar.edu; rotman1@llnl.gov)

[1]Also at Science Systems and Applications,

Inc., Lanham, Maryland

[2]Now at NASA Langley Research Center,

Hampton, Virginia.

[3]Now at National Center for Atmospheric

Research, Boulder, Colorado.

Abstract.

A model intercomparison among the Atmospheric and Environmental Research (AER) 2-D model, the Goddard Space Flight Center (GSFC) 2-D model, and the Lawrence Livermore National Laboratory (LLNL) 2-D model allows us to separate differences due to model transport from those due to the model's chemical formulation. This is accomplished by constructing two hybrid models incorporating the transport parameters of the GSFC and LLNL models within the AER model framework. By comparing the results from the native models (AER and e.g. GSFC) with those from the hybrid model (e.g. AER chemistry with GSFC transport), differences due to chemistry and transport can be identified. For the analysis, we examined an inert tracer whose emission pattern is based on emission from a High Speed Civil Transport (HSCT) fleet; distributions of trace species in the 2015 atmosphere; and the response of stratospheric ozone to an HSCT fleet. Differences in NO_y in the upper stratosphere are found between models with identical transport, implying different model representations of atmospheric chemical processes. The response of O_3 concentration to HSCT aircraft emissions differs in the models from both transport-dominated differences in the HSCT-induced perturbations of H_2O and NO_y as well as from differences in the model representations of O_3 chemical processes. The model formulations of cold polar processes are found to be the most significant factor in creating large differences in the calculated ozone perturbations.

1. Introduction

Studies have shown that transport is a major uncertainty in 2-D and 3-D modeling of the atmosphere [*Jackman et al.*, 1991; *Kinnison et al.*, 1994; *Douglass et al.*, 1999]. Models also differ in their treatment of chemistry. Though most models employ the chemical reaction rates from JPL [*DeMore et al.*, 1997; *Sander et al.*, 2000], differences exist in family groupings, diurnal averaging technique, and treatment of heterogeneous chemistry. Calculations of ozone perturbations by different models show differences which are not easy to interpret. How much of these differences are due to differences in transport? How much to differences in chemistry? Better understanding of intermodel differences would help in placing uncertainty estimates around model predictions of future ozone changes.

Model intercomparisons have typically involved comparisons of spatial and temporal distributions of trace gases. Information on differences in chemistry is obtained by comparing radical concentrations calculated using specified long-lived species concentrations (see e.g. the chemistry intercomparison exercises in M&M I [*Prather and Remsberg*, 1993] and M&M II [*Park et al.*, 1999]). Intercomparisons of model dynamics use idealized tracer species calculated with prescribed production and loss rates. Tracer concentrations are then compared, or quantities such as age of air are derived from the tracer mixing ratios [*Hall et al.*, 1999; *Park et al.*, 1999].

This paper will employ a different approach. This study is based on three two-dimensional (2-D) models: the Atmospheric and Environmental Research (AER) 2-D model, the Goddard Space Flight Center (GSFC) 2-D model, and the Lawrence Livermore National Laboratory (LLNL) 2-D model. The transport parameters, and to the extent possible, the numerical scheme and grid resolutions of the LLNL and GSFC models

have been implemented within the AER model. Using this approach, chemical differences for both long- and short-lived species can be evaluated by comparing two models with similar transport but different chemical formulations. The effect of transport on model-calculated perturbations can be evaluated by comparing results from the AER model with different transport formulations but identical chemistry. This modular approach to model intercomparison is being used in the 3-D Global Modeling Initiative (GMI) model [*Douglass et al.*, 1999; *Considine et al.*, 2000; *Rotman et al.*, 2001; *Kinnison et al.*, 2001].

The following section will describe the dynamical and chemical formulations of the three models. Section three will describe the intercomparison approach used. Section four will present an intercomparison of a background atmosphere calculation for 2015 conditions. Section five will present an intercomparison of calculated perturbations to H2O, NO_y, and ozone due to a future fleet of stratospheric aircraft. Section six includes discussion and conclusions. It should be noted that the results presented in the paper were generated by the models around 1997 in preparation for the M&M II [*Park et al.*, 1999] and *IPCC* [1999] reports. Each model has continued its modifications and refinements since then. Although many details of the results presented in this paper may well have been superseded by later work, this in-depth comparison of three 2-D models provides insights into many intermodel differences. This paper also presents a demonstration of a new capability for comparing different 2-D model results, in which one of the models provides the framework for inclusion of the advection and diffusion of other models.

2. Model Descriptions

The three models considered here differ substantially in model formulation and details of chemistry and dynamics. All three models use log pressure as the vertical coordinate,

but vertical resolution varies from 1.2 km in the AER model to 1.5 km in the LLNL model to 2.0 km in the GSFC model. The GSFC model uses 10 degree horizontal resolution, the AER model 9.5 degree horizontal resolution, and the LLNL model 5 degree horizontal resolution. The top of the GSFC model extends to 90 km, the LLNL model to 80 km, and the AER model only to 60 km. All three models use observed climatological temperatures taken from NCEP analyses [*Kalnay et al.*, 1996].

2.1. Transport Parameters

The transport coefficients of the LLNL model [*Kinnison et al.*, 1994; *Li et al.*, 1995] are computed using model-calculated ozone and observed temperatures. Mechanical forcing from planetary waves breaking (represented explicitly by two waves), gravity wave breaking, and Rayleigh friction are also employed. While this calculation is done interactively in the original LLNL model, the transport parameters from a previous calculation have been saved and used repeatedly in the LLNL results and the hybrid model calculations presented here. The horizontal diffusion K_{yy} is calculated as the ratio of the E-P flux divergence to the gradient of potential vorticity [*Garcia*, 1991], with a minimum value set at $1x10^8$ cm^2/s in the stratosphere. Tropospheric K_{yy} is set to $1x10^{10}$ cm^2/s. A gravity wave breaking parameterization is used to calculate K_{zz} in the stratosphere, with values ranging from $2x10^3$ cm^2/s to over $1x10^5$ cm^2/s. K_{zz} in the troposphere is set to $4x10^4$ cm^2/s. Figure 1 shows K_{yy} and vertical velocity from the LLNL model for June and December. Note the large gradients in the K_{yy} fields, especially in December where values of the equatorial K_{yy} exceed $40x10^{10}$ cm^2/s near 40 km.

The GSFC model (see *Jackman et al.* [1996]; *Fleming et al.* [1999]) calculates transport parameters from observed climatological values of temperature, H_2O, zonal wind

and ozone. Mechanical forcing from six planetary waves (constructed from the observed temperature field) and effects of gravity wave breaking provide the wave driving. The diabatic heating rates are computed following *Rosenfield et al.* [1994], and latent heating in the troposphere is taken from *Newell et al.* [1974]. The streamfunction is obtained by solving an elliptic equation obtained by combining the zonal-mean momentum and energy equations (see e.g., *Garcia and Solomon* [1983]). K_{yy} is computed using a similar theoretical basis as that used by the LLNL model but employing observed meteorological data and following the approach of *Randel and Garcia* [1994]. K_{yy} values range from $1x10^8$ to $5x10^{10}$ cm^2/s, with values computed in both troposphere and stratosphere. K_{zz} values in the troposphere and lower stratosphere are based on the vertical temperature gradients. In the upper stratosphere and mesosphere, K_{zz} values are obtained from a gravity wave parameterization. Stratospheric values of K_{zz} range from $1x10^2$ cm^2/s in the lowermost stratosphere to $5x10^5$ cm^2/s in the upper stratosphere. Tropospheric values of K_{zz} range from $1x10^4$ cm^2/s at the tropopause to $5x10^5$ cm^2/s at the surface in the tropics and $2.5x10^5$ cm^2/s at the surface near the poles. Figure 2 shows K_{yy} and vertical velocity for June and December from the GSFC model.

The AER model uses transport parameters obtained in a more ad hoc manner than the GSFC or LLNL models. Heating rates, based loosely on Dopplick [1979], are scaled by temperature lapse rate and used to obtain the vertical velocity. The vertical velocity field is integrated to obtain a streamfunction, with adjustments made to assure mass conservation (see *Ko et al.* [1985]). Diffusion rates are specified independently of the advective circulation, with K_{yy} values in the lower stratosphere based on studies of exchange time scales between the tropics and midlatitudes [*Shia et al.*, 1998]. Values chosen are from 0.7-

1.3x10^9 cm^2/s in the tropics and from 3-10x10^9 cm^2/s elsewhere. K_{zz} values are constant at 1x10^5 cm^2/s in the troposphere, 1x10^3 cm^2/s in the lower and middle stratosphere, and 1x10^4 cm^2/s in the upper stratosphere. K_{yz} values are obtained by projecting the K_{yy} values from isentropic surfaces to pressure surfaces. There has been no attempt to maintain consistency between the advective and diffusive components of transport within the AER model. Figure 3 shows K_{yy} and vertical velocity for June and December from the AER model. The parameterized K_{yy} values shown are constant for six months of the year, changing in April and October.

The LLNL model shows the strongest Hadley circulation in the troposphere. The GSFC model has a weak Hadley circulation, and the AER model has none. The GSFC circulation is the weakest overall in the stratosphere. The AER model has consistently the largest diffusion coefficients. Mean age of air calculated from the models reflects both advective and diffusive transport and can be compared with age fields derived from observations. The GSFC model has the longest age of air in the upper stratosphere, with LLNL significantly shorter and AER shortest as reported in the M&M II report [*Park et al.*, 1999]. Since most 2-D models generate age of air which is shorter than observations indicate, the GSFC model is most realistic in this regard.

2.2. Diurnal Treatment and Time Stepping Scheme

The approaches for dealing with time stepping and diurnal variability differ in significant ways among the three models. The AER and GSFC models use a family approach and transport only long-lived species, whereas the LLNL model does explicit time stepping of all species. The GSFC model transports the species N_2O_5 and $ClONO_2$ which the AER model considers part of the NO_y and/or Cl_y families. Since zonal mean quantities

are transported in 2-D models, the zonal mean production and loss rates are used in the mass-continuity equation for long-lived species. Different techniques are used to obtain the zonal-mean production and loss rates. These involve first calculating the diurnal variations in the radical species.

Computation of radical species in the AER model is performed with 17 explicit time steps over the diurnal cycle. Production and loss rates of long-lived species are computed from the radical concentrations at each of the 17 time steps and averaged over 24 hours. New production and loss rates are computed daily. The Smolarkiewicz scheme [*Smolarkiewicz,* 1984] is used for time stepping of advection. The rates of change due to chemistry, diffusion, and advection are used to update long-lived species with a time step of 6 hours using an explicit scheme.

The GSFC model does explicit diurnal calculations only for those radical species which are produced at night, ie. HNO_3, NO_2, NO_3, N_2O_5, HOCl, HCl, ClO, $ClONO_2$, BrO, HOBr, and $BrONO_2$. For other species, daytime average photolysis rates are used, along with dawn values of the night species, to calculate daytime average radical concentrations and production and loss rates for long-lived species. Time stepping of long-lived species is done with split operators, using a 12 hour time step for advection, a 3 hour step for vertical diffusion, a 24 hour step for horizontal diffusion, and a 24 hour step for chemistry. The Lin and Rood scheme [*Lin and Rood,* 1996] is used for advective transport.

The LLNL model does explicit diurnal chemistry for all species with 15 minute time steps for chemistry and 2 hours time steps for transport, time marching 2 days at a time for each process. The Smolarkiewicz scheme is used for advection. To save computer time,

the diurnal version is run for one year while saving diurnal averaging coefficients daily. Then the diurnal average version of the model is run for two years using these coefficients.

2.3. Chemistry Content

Each model uses the JPL-97 compendium [*DeMore et al.*, 1997] as the source of reaction rate data. The monthly mean zonal mean temperature from climatology is used to calculate the rate constants for gas-phase reactions. Six heterogeneous reactions on sulfate aerosol are employed in each model. Aerosol surface area is specified in these calculations, so reaction rates on sulfate aerosol are the same for all three models except for the way temperature variation is included in the rate calculation. Both LLNL and AER utilize a temperature distribution taken from NCEP reanalysis data [*Kalnay et al.*, 1996] which accounts for longitudinal and day-by-day deviations of temperature from the monthly zonal mean temperature. The reaction probability and the molecular thermal velocity are evaluated at each temperature in the distribution and then the mean value of the product is used, along with the aerosol surface area, to obtain the zonal mean reaction rate. This methodology is found to make a significant difference in reaction rates for those reactions which are strongly temperature dependent ($ClONO_2$ + H_2O, $BrONO_2$ + H_2O, $ClONO_2$ + HCl) [*Weisenstein et al.*, 1998; *Pitari*, 1993]. The GSFC model employs only the zonal mean temperature in the rate calculation for sulfate aerosols.

Various intercomparison exercises have demonstrated that standard application of Beer's law to account for O_2 and O_3 absorption in photolysis calculations provides reliable results in most cases. Care must be used, however, in the Schumann-Runge (S-R) bands for O_2 photolysis and NO absorption. The AER model uses the photolysis code of Michael Prather [*Prather*, 1993] which handles the S-R bands according to *Minschwaner*

et al. [1992]. The online photolysis calculation includes the effects of Rayleigh scattering in a spherical atmosphere. The attenuated flux in 77 wavelength bands at each grid point is calculated and multiplied by the molecular cross sections obtained from *DeMore et al.* [1997]. Photolysis rates or J-rates are the integral of this product over wavelength, and are calculated for the ten daytime time points. Photolysis rates for O_2 and NO are calculated separately to account for the fine structure of the S-R bands.

The GSFC model uses a lookup table for the photolytic source term (PST) and photolysis of O_2 [$J(O_2)$]. This table was generated by R. Kawa (GSFC) using a radiation code developed by D. Anderson and coworkers at the Johns Hopkins University Applied Physics Laboratory [*Anderson and Meier,* 1979; *Anderson and Lloyd,* 1990]. The PST and $J(O_2)$ table is given on the pressure grid of the GSFC 2-D model and is a function of wavelength, solar zenith angle and column ozone. The PST is computed for the particular wavelength, solar zenith angle, column ozone, and pressure of interest and is multiplied by the solar irradiance at the top of the model to compute the flux at the point of interest. The flux is then used with the photodissociation cross section for a particular constituent to derive the photolysis rate of interest.

The lookup table used in the LLNL model is a derivative of the GSFC lookup table described above. The PST was generated at each of 79 wavelengths for LLNL by R. Kawa (GSFC) using the radiative transfer code mentioned above for 35 pressure levels, 20 solar zenith angles, and 12 overhead ozone columns with varying range appropriate to the associated pressure. Molecular cross sections for photolysis for the same wavelength bin structure were determined from laboratory sources [*DeMore et al.*, 1997], at 200 values of local temperature, covering the range encountered in the atmosphere. The J

values are then determined on-the-fly by integrating, over wavelength, the product of the exoatmospheric flux, the interpolated PST, and the actinic cross section at the current local temperature. Because evaluation of $J(O_2)$ requires treatment of the S-R bands, LLNL interpolated $J(O_2)$ from the GSFC values as a function of pressure, solar zenith angle, and overhead ozone column, rather than by integration over the wavelength bins in the model.

All three models include lightning as a source of NO_y in the tropical troposphere, with the AER and GSFC models assuming a source strength of 2 megatons per year distributed from 4 to 14 km in altitude. The LLNL model assumes a source strength of 5 megatons per year distributed according to the ISCCP cloud database [*Rossow and Schiffer*, 1999]. Some species are removed in the troposphere through rainout/washout processes in each of the models, though both the rates of these processes and the species subject to washout vary somewhat from model to model. All three models remove H_2O_2, HNO_3, HCl, and HBr. In addition to the common set, the GSFC model also removes HO_2NO_2, CH_3OOH, HF, CClFO, and CF_2O; the AER model also removes CH_3OOH, CH_3O_3H, CH_2O, HF, and CF_2O; and the LLNL model also removes N_2O_5, HO_2NO_2, CH_2O, ClO, HOCl, $ClONO_2$, and $BrONO_2$. Washout rates in the LLNL model vary from 3 days in the lowest 4 km to 50 days near the tropopause. The AER model uses similar washout rates (5 days near the surface to 40 days at 10 km), but with no washout above 10 km. The GSFC model used the slowest washout rates: from 25 to 100 days.

Distributions of H_2O in the troposphere are based on prescribed relative humidity values in the AER and LLNL models. In addition, the AER model specifies the water vapor mixing ratio just above the tropopause (2.75 ppmv in the tropics, up to 3.5 ppmv at high

latitudes). The GSFC model specifies water vapor below 400 mb based on the climatology of *Oort* [1983]. Water vapor is transported in the troposphere above 400 mb in the GSFC model, with H_2O concentrations in excess of 50% relative humidity rained out [*Fleming et al.*, 1995]. All three models calculate H_2O concentration in the stratosphere using appropriate chemical sources (including methane oxidation) and sinks.

2.4. Polar Heterogeneous Chemistry Formulation

Though gas-phase reaction rates of stratospheric interest have been fairly well standardized by the JPL compendium [*DeMore et al.*, 1997], treatment of heterogeneous chemistry, particularly under cold polar conditions, differs greatly between models. Approaches include assuming nitric acid trihydrate (NAT), sulfuric acid trihydrate (SAT), or supercooled ternary solution (STS) compositions for type I polar stratospheric cloud (PSC) particles. Some models calculate PSC surface area based on model calculated HNO_3 and H_2O, while others base PSC surface area on observations. Some models account for sedimentation of PSC particles, while others assume a fixed rate of denitrification under certain conditions. Two-dimensional models in addition need to account for the zonal asymmetry of temperature. Since there is no consensus on how best to represent cold polar processes, the GSFC, LLNL, and AER models implement different approaches.

Both GSFC and AER employ thermodynamic equilibrium parameterizations to calculate Type I (assumed to be NAT) and Type II (ice) PSCs based on available gas phase H_2O and HNO_3 and a distribution of temperatures. The GSFC model assumes that supersaturation factors of 10 for NAT and 1.4 for ice are required before PSCs form. The AER model assumes no supersaturation. The GSFC model assumes lognormal size distributions of PSC particles, with NAT having a mode radius of 1.0 μm and a σ of 1.8 and ice

particles having a mode radius of 10 μm and a σ of 1.8 [*Considine et al.*, 1994]. The AER model assumes a single radius for each type of particle, 0.5 μm for NAT and 7 μm for ice. Because of the particle size assumptions, the GSFC model has greater sedimentation and denitrification/dehydration. The temperature distribution is applied only to obtain the PSC surface area in the GSFC model, while the AER model applies the temperature distribution to obtain the product of the reaction rate and surface area.

The LLNL model handles cold heterogeneous processes by assigning a supercooled ternary solution (STS) composition to PSC particles. The particle surface area is not calculated by the model. Instead, a surface area density of 1 $\mu m^2/cm^3$ is imposed within 25° of the poles when the PSC climatology of *Poole and Pitts* [1994] indicates a PSC frequency of occurrence exceeding 0.08. Reaction rates are obtained by integrating over the temperature distribution and then multiplying by the fixed PSC surface area. Dehydration and denitrification are represented globally (independent of the PSC surface area parameterization) by assuming that the partial pressure in excess of the saturation vapor pressure over ice (calculated using zonal mean temperatures) is removed permanently with first order time constants of 1 day for H_2O and 0.5 days for HNO_3.

3. The Hybrid Models

3.1. Approach

Transport parameters from the GSFC and LLNL models were used in the AER model. The version of the AER model with GSFC transport coefficients will be referred to as the AER/GSFC model. The version of the AER model with LLNL transport coefficients will be referred to as the AER/LLNL model. The streamfunction can be interpolated to different grid resolutions while maintaining a nondivergent flow field. The horizontal and

vertical diffusion fields, K_{yy} and K_{zz}, are also used and can be interpolated between grids if necessary. The GSFC and LLNL models do not use a K_{yz} field, so K_{yz} is set to zero in the hybrid models.

The transport algorithms and numerics of the AER model were modified to some extent for the hybrid models. It was found necessary to use the LLNL grid (5° latitude, 1.5 km vertical) within the AER/LLNL model when using the LLNL transport parameters because of sharp gradients in the LLNL diffusion fields. The AER/LLNL model was also modified to use the same time splitting scheme for the advective and diffusive time steps as the LLNL model. Since the AER and LLNL models both use the Smolarkiewicz transport scheme, the transport algorithm was not modified. The top boundary of the AER/LLNL model was set at 80 km as in the LLNL model.

The GSFC model uses the *Lin and Rood* [1996] scheme for transport. We decided that it was not practical to modify the transport scheme for the AER/GSFC model, so it uses Smolarkiewicz like the AER model. We ran the AER/GSFC model in the original GSFC grid resolution and in the AER grid resolution. In both cases, differences with the GSFC model were found due to the different transport scheme, and the grid resolution made only a small additional difference. Therefore we opted to employ the AER model grid resolution in the AER/GSFC results presented here. Note that the top boundary of the AER/GSFC model is 60 km, not 90 km as in the GSFC model.

The hybrid models use the chemistry formulation of the AER model, including the photolysis scheme, reaction rates, and heterogeneous chemistry formulation for sulfate and PSCs. The family approach and diurnal calculations of the AER model are retained in the hybrids. The hybrid models thus represent the AER model's chemistry with dynamics

replaced by those of another model. The following inert tracer experiment is used to test whether the LLNL and GSFC transport formulations have been implemented correctly within the hybrid models, and how closely the implementation matches the native model.

3.2. Inert Tracer Comparison

The Models and Measurements II experiment A-3 [*Park et al.*, 1999] is used to test the accuracy of the GSFC and LLNL transport implementation within the AER model. This experiment is designed to mimic the NO_y perturbation due to a fleet of 500 supersonic aircraft cruising at Mach 2.4. with most emissions occurring in the northern hemisphere at altitudes of 18-20 km. The source is taken from the 1995 NASA HSCT scenario [*Stolarski et al.*, 1995] with NO_x emissions of 10 grams NO_2 per kilogram of aircraft fuel burned. Removal in the troposphere is simulated by setting a boundary condition of zero concentraiton below 6 km. There is no stratospheric removal.

June results of the inert tracer calculation from the AER, AER/GSFC, AER/LLNL, GSFC, and LLNL models are shown in Figure 4. Comparison of the results from the native models (panels a, d, and e) shows that the GSFC model retains the most emitted material in the stratosphere (80% more than the AER model and 65% more than the LLNL model). Consequently the GSFC model transports the most tracer to the upper stratosphere and the southern hemisphere (by more than a factor of two). When these results are scaled to represent equal atmospheric burdens of injected tracer, the GSFC model obtains 18% more tracer at 45°S and 20 km than the AER model and 29% more than the LLNL model, indicating that the models differ in their global distribution of tracer. Differences between the native model and the corresponding hybrid model reflect the extent to which the hybrid model transport does not reproduce the native model.

Differences between the GSFC and AER/GSFC models are 4-6% above 20 km and much larger near the tropopause (up to a factor of two). The comparison between the LLNL and AER/LLNL models shows differences of only 1-3% everywhere.

Differences between the GSFC and AER/GSFC models are likely due largely to the difference in the transport schemes, *Smolarkiewicz* [1984] for the AER model and *Lin and Rood* [1996] for the GSFC model. The difference in transport schemes is especially noticeable near the tropopause where gradients are large. Note that the AER/GSFC model results were obtained with the GSFC transport parameters interpolated to the AER grid. Performing the calculation on the GSFC grid in the AER/GSFC model results in only slightly better agreement. The LLNL and AER/LLNL models both use the Smolarkiewicz transport scheme and show minor differences. We attribute these differences to minor differences in the model numerics and the Smolarkiewicz implementation. This set of exercises assures us that the hybrid models provide a good approximation of the transport properties of the native models.

4. Background Atmosphere Intercomparison

We now use the results from the hybrid models to illustrate how they can help to explain the differences in simulated distributions of chemical species in the atmosphere. The background atmosphere is obtained from the Atmospheric Effects of Aviation Program (AEAP) calculations that corresponds to a 2015 atmosphere with subsonic aircraft [*IPCC*, 1999; *Kawa et al.*, 1999], and is labeled scenario D in the *IPCC* [1999] calculations. The 2015 atmosphere is assumed to contain a stratospheric Cl_y concentration of 3.0 ppbv, N_2O surface concentration of 330 ppbv, and background (nonvolcanic) levels of stratospheric aerosol.

Each of the calculations presented represents the model's steady-state condition, i.e. there is no appreciable change in the species' concentrations from one year to the next. Because of the uncertainties associated with PSC chemistry, two simulations were performed for each model: one with and one without PSC chemistry. The model results are discussed in the following format. Figure 5 shows the distributions of NO_y, H_2O, Cl_y, and O_3 from the AER model in October with the PSC parameterization. The differences among models are discussed using Figures 6-15. In these figures, panels (a), (b) and (c) show the differences in calculated concentrations for cases with a PSC parameterization between the models for (X-AER), (AER/X-AER), and (X-AER/X) respectively, where X represents either GSFC or LLNL and AER/X is a hybrid model. Note that algebraically, the sum of the differences in panels (b) and (c) equals the difference in panel (a). The difference in panel (b) is due to differences in transport parameters (winds and eddy diffusion coefficients). The difference in panel (c) is mostly due to differences in chemical formulation. However, differences in numerical treatment and time-stepping also contribute. Panel (d) shows the difference (X-AER/X) without the PSC parameterization. Comparison of panels (c) and (d) isolates the difference due to PSC treatment.

It is not the purpose of this study to compare the model results with observations. In fact, use of the 2015 background atmosphere makes observational comparisons impossible. It is useful to keep in mind, however, that the AER model tends to calculate too low a concentration in the lower stratosphere for downward diffusing species (eg. O_3, NO_y, Cl_y). Compared with the TOMS climatology, the AER model calculates too much ozone during the springtime maximum (by about 10%-15%), and underpredicts ozone column at the tropics by about 5%-10%.

4.1. NO_y

Figure 5a shows the distribution of total odd nitrogen (NO_y) calculated by the AER model for October. A maximum value of 20 ppbv is calculated in the tropics at around 40 km, falling off to 10 ppbv at 50km and 30 km. At higher latitudes, the maximum NO_y value (about 15 ppbv) is found near 30 km. The GSFC and LLNL native models (Figures 6a and 7a) calculate more NO_y than the AER model (by as much as 12 ppbv in the upper stratosphere). Transport differences (shown in Figures 6b and 7b) lead to relatively large differences (both positive and negative, up to 6 ppbv) in concentration in the upper stratosphere and tropical mid stratosphere as well. With the premise that the hybrid models mostly remove the effects of different transport, the differences shown in Figures 6c and 7c should be the result of different chemistry. For NO_y, this would mean the source terms from N_2O and lightning, the gas-phase removal term by photolysis of NO, removal by PSC chemistry, and washout in the troposphere. Results from Figures 6d and 7d show that the effect of PSCs is limited to near the poles at 10-25 km altitude. The upper stratospheric chemical difference is likely due to differences in NO photolysis.

4.2. H_2O

Figure 5b shows the gas-phase H_2O distribution calculated by the AER model for October. Figure 8a shows that the GSFC model calculates up to 1 ppmv more H_2O in the lower and middle stratosphere. Figures 8b and 8c suggest that most of the difference in the lower stratosphere is due to the difference in the tropospheric boundary condition. However, the transport difference is still responsible for half the difference in some regions of the middle stratosphere. The LLNL model also calculates more H_2O (Figure 9a) in the lower stratosphere and much of the middle stratosphere. In this case, transport differences

are generally larger than the chemical differences, but of opposite sign. Figures 8d and 9d show that differences in PSC treatments have a small effects in both cases.

4.3. Cl_y

The distribution of total inorganic chlorine (Cl_y) calculated by the AER model for October is shown in Figure 5c. The differences among the native models (Figures 10a and 11a) in the upper stratosphere are less than 5%. This shows that each model achieves an inorganic chlorine content in the upper stratosphere roughly equal to the input of organic chlorine in the troposphere. The differences are much larger in the lower stratosphere, approaching a factor of 2. Transport is responsible for the bulk of the differences (Figures 10b and 11b). However, Figures 10c and 11c still show differences due to chemistry, which can be attributed to differences in washout and details of the numerical schemes (which affect the simulation of transport in regions with large gradients such as the tropopause). PSC treatments have a negligible effect on Cl_y.

4.4. Ozone

Figure 5d shows the O_3 distribution calculated by the AER model for October. The native GSFC (Figure 12a) and LLNL (Figure 13a) models show less O_3 (by as much as 15% or 1.5 ppmv) than the AER model in the equatorial middle stratosphere and the midlatitude lower to middle stratosphere. About 2/3 of the difference in the tropics is due to transport and the remainder due to chemistry (see Figures 12b,c and 13b,c). In the southern high latitudes in October, chemistry accounts for most of the difference between the AER and GSFC models, specifically the PSC treatment (as can be seen by comparing Figures 12c and d). The comparison between the AER and LLNL models in the southern

high latitudes shows that effects of transport and chemistry partially cancel each other in October, with transport having a somewhat larger effect.

The results from comparisons of calculated ozone column are given in Figures 14 and 15. Both the GSFC and the LLNL models calculate more O_3 in the tropics and less O_3 at high latitudes than the AER model (generally resulting in better agreement with TOMS observations). The LLNL model also calculates more O_3 in the midlatitudes than the AER model. Both chemistry and transport play significant roles in the differences, often with competing effects. In the southern hemisphere high latitudes, the GSFC model calculates 20-100 DU less than the AER model. Transport differences between the AER and GSFC models produce more ozone in austral summer and less in austral winter. In the absence of PSCs (see Figure 14d), chemical differences account for a difference of less than 20 DU. Inclusion of PSCs in the models greatly reduces the ozone column in the GSFC model relative to the AER model. In the AER-LLNL model comparisons, transport leads to lower ozone columns at high southern latitudes for LLNL, while chemistry leads to higher ozone columns in the same region. Without PSCs in either model, chemical differences are less than 10 DU. The LLNL model has the least efficient PSC mechanism for depleting ozone and the GSFC model the most efficient scheme.

5. Intercomparison of Calculated HSCT Perturbations

Over the past few decades there has been much interest in a potential fleet of commercial supersonic aircraft and its atmospheric impact. There have been numerous modeling studies to investigate the impact of High Speed Civil Transport (HSCT) aircraft in the lower stratosphere and upper troposphere [*IPCC*, 1999; *Kawa et al.*, 1999; and references therein]. These studies consist of various scenarios used to explore the effects of parametric

modifications in the HSCT aircraft fleet size, cruise altitude, emission parameters, and the background atmosphere. The model response can be generally explained in terms of the amount of engine emissions retained in the stratosphere (a transport issue), and the response of ozone to these perturbations (where both transport and chemistry play a role). It is the latter complication that makes it difficult to separate the two effects and intercompare model results in a meaningful way.

To make use of existing computations, we used results from the *IPCC* [1999] exercise, in which the AER, GSFC and the LLNL models participated, and generated additional results with the AER/GSFC and the AER/LLNL hybrid models. We have chosen to examine scenario S1c from *IPCC* [1999], which includes a fleet of 500 HSCT aircraft operating in 2015, with a NO_x emission index of 5 grams of NO_2 per kilogram of fuel burned and H_2O emission index of 1230 grams per kilogram of fuel. The aircraft have a cruise altitude of 18-20 km and fly predominately in the northern hemisphere. This scenario is compared with Scenario D discussed in section 4 which represents a 2015 background atmosphere with only subsonic aircraft.

Scenario S1c was calculated by nine modeling groups for the *IPCC* [1999] assessment report. Annual average ozone column perturbations ranged from 0.0% to -0.4% for the northern hemisphere and from 0.0% to -0.8% for the southern hemisphere [*IPCC*, 1999]. This large difference in ozone response is difficult to interpret without a complete understanding of the model differences. By examining perturbations of O_3 column, local O_3, H_2O, and NO_y using the AER/GSFC and the AER/LLNL hybrid models, we can obtain an understanding of how the different model chemical formulations affect the ozone perturbations. This, in turn may provide a better understanding of the variability in

the calculated ozone perturbations from different modeling groups. We will first discuss calculations without PSC chemistry, to simplify the interpretation. We will then show O_3 perturbation results with PSC chemistry, which has quite a large impact on these calculations.

Perturbations to H_2O are shown in Figure 16 for October without PSC chemistry. Perturbations to NO_y are shown in Figure 17 for the same conditions. The H_2O results are similar to those for the inert tracer shown in Figure 4 when scaled for emissions (factor of 0.31). The NO_y results should scale by 0.5 from results shown in Figure 4 except that NO_y has chemical loss in the upper stratosphere. As in experiment A-3, more of the emissions are transported to the southern hemisphere in the GSFC model than the AER or LLNL models. The HSCT NO_y and H_2O perturbation differences between the native models and the hybrid models are fairly small, despite the fairly large differences between the NO_y and H_2O background concentrations, indicating that transport plays the major role for these gases.

Perturbations in O_3 for October due to HSCT emissions are shown in Figure 18 for simulations without PSC chemistry. The GSFC and AER/GSFC models show twice as much O_3 depletion in the upper stratosphere as the other models due to having twice the H_2O perturbation in this region. Models with similar transport show similar ozone depletion in the upper stratosphere, but somewhat different ozone perturbations in the lower stratosphere. These differences could be due to the different background levels of NO_y, Cl_y, Br_y, and H_2O in this region or to different chemical treatment of O_3. Differences in transport (compare panels a, b, and c) have a large impact on the calculated O_3 perturbation near the tropopause at mid and high latitudes. Figure 19 shows perturbations in

O_3 column for simulations without PSC chemistry. Of the native models, AER and LLNL show only 0.1% O_3 depletion in the southern tropics, while the GSFC model shows 0.3% O_3 depletion here. The LLNL model shows the greatest O_3 depletion at both poles. The GSFC model shows the least depletion at the north pole, but the most at 30°N.

The seasonal variability at high latitudes seen in the AER model is reflected in the hybrid models as well, indicating that this feature is due to the chemical scheme in the AER model and not due to transport. The LLNL model calculates much more O_3 depletion in the high southern latitudes than the AER/LLNL model. Background concentrations of NO_y in the high latitude lower stratosphere are much larger in the LLNL model than the AER/LLNL model and background H_2O concentrations are lower, which would result in more sensitivity to NO_y perturbations in the LLNL model. The GSFC and AER/GSFC models both show a maxima of O_3 depletion at 30°N, indicating that this is a feature of the GSFC transport (a result of the O_3 enhancement from 40-90°N at 8-12 km altitude seen in Figure 18). However, the AER/GSFC model shows a maximum of O_3 depletion at the north pole, especially in springtime, whereas the GSFC model shows a minimum here.

With PSC chemistry, all models show denitrification and dehydration at the south pole in austral spring. The GSFC model, but not the AER or LLNL models, also shows denitrification near the north pole in springtime. This is due to the different ways that NAT particle sizes are specified in the models, resulting in more particle sedimentation in the GSFC model. O_3 perturbations for October with PSC chemistry are shown in Figure 20, and perturbations in O_3 column are shown in Figure 21. All models show enhanced O_3 depletion in both hemispheres with PSC chemistry included, except for the

LLNL model in the northern hemisphere. PSC chemistry has a very large impact on calculated ozone perturbations due to HSCT at high latitudes and increases the model differences. The hybrid models show much more O_3 depletion at high northern latitudes than the GSFC and LLNL models, though the GSFC model shows more depletion than the AER/GSFC model in the southern high latitudes.

6. Discussion and Conclusions

Traditional comparisons of model-calculated ozone perturbations are incomplete because reasons for the model differences cannot be diagnosed. We have approached this problem by constructing hybrid models which employ the transport fields of one model within the framework of another model. We demonstrate that the use of hybrid models can help to separate, to a large extent, the effects of transport and chemistry on model calculated results. The intercomparison performed in this study has lead to improvements in the participating models. Because of the NO_y comparison problem identified in this study, the LLNL model has modified J(NO) by creating a new lookup table for this parameter derived from AER results (ie. the UCI photolysis code) calculated for January and July, used by interpolation to the appropriate pressure, solar zenith angle, and overhead ozone column.

The inert tracer results in section 3.2 show that the native models' advective winds and eddy coefficients accounts for the bulk of the transport differences, although the numerical scheme still has a small effect. The comparisons of the background atmosphere indicate that the tropospheric boundary condition for H_2O has a large effect on the model calculated stratospheric distribution. The very large difference in NO_y in the middle and upper stratosphere can probably be attributed to treatment of the NO photolysis rate.

The choice of transport parameters has a substantial effect on model calculated NO_y, Cl_y and H_2O in the lower and middle stratosphere, with both positive and negative differences seen. Differences in ozone are the result of differences in NO_y, Cl_y, Br_y, and H_2O caused by both chemistry and transport, as well as differences in transport of ozone itself. PSC parameterizations represent a large difference in model formulations, and this is evident in the ozone comparisons.

In the HSCT perturbation calculations, our results showed that most of the differences in the H_2O and NO_y perturbations are due to transport. Calculated ozone differences in the upper stratosphere can be attributed to differences in transport of H_2O. Differences in the lower stratosphere are more difficult to interpret, but high latitude ozone behavior appears to be controlled by chemistry to a greater extent than midlatitude ozone. When PSC processes are omitted from the models, differences in ozone column perturbation between models with the same transport are fairly small (less than 0.2% in most regions). When PSC processes are included, differences can be as high as 1% at high latitudes. For models with identical chemistry but different transport, differences in ozone column perturbation due to HSCT are no larger than 0.3% when PSC processes are omitted. Including PSCs yields differences in ozone column perturbation of up to 1.6% between models with identical chemistry.

This study has allowed us to quantitatively diagnose transport differences between three of the models used in the IPCC assessment of supersonic aircraft [*IPCC*, 1999]. It is well known that differences in model transport play a major role in calculated ozone perturbation differences. A more surprising result is that differences in model chemical treatment produce significant differences in perturbation results as well, despite the fact

that all models use the same set of reaction rate coefficients. These differences are much larger when PSC processes are included in the models. As more is learned about the formation of PSCs in the future, it is hoped that model treatment of these processes will become more standardized and this source of model discrepancy reduced.

Acknowledgments.

This work was supported by the NASA Atmospheric Chemistry Modeling and Analysis Program and the NASA Atmospheric Effects of Aviation Project. Portions of this work were performed under the auspices of the U.S. Department of Energy by the University of California Lawrence Livermore National Laboratory under contract No. W-7405-Eng-48.

References

Anderson, D. E., Jr., and R. R. Meier, Effects of anisotropic multiple scattering on solar radiation in the troposphere and stratosphere, *Appl. Opt., 18,* 1955-1960, 1979.

Anderson, D. E., Jr., and S. A. Lloyd, Polar twilight UV-visible radiation field: Perturbations due to multiple scattering, ozone depletion, stratospheric clouds, and surface albedo, *J. Geophys. Res., 95,* 7429-7434, 1990.

Considine, D. B., A. R. Douglass, and C. H. Jackman, Effects of a polar stratospheric cloud parameterization on ozone depletion due to stratospheric aircraft in a two-dimensional model, *J. Geophys. Res., 99,* 18,879-18,894, 1994.

Considine, D. B., A. R. Douglass, P. S. Connell, D. E. Kinnison, and D. A., Rotman, A polar stratospheric cloud parameterization for the three dimensional model of the global modeling initiative and its response to stratospheric aircraft, *J. Geophys. Res., 105,* 3955-3975, 2000.

Douglass, A. R., M. P. Prather, T. M. Hall, S. E. Strahan, P. J. Rasch, L. C. Sparling, L. Coy, and J. M. Rodriguez, Choosing meteorological input for the global modeling initiative assessment of high speed aircraft, *J. Geophys. Res., 104,* 27545-27564, 1999.

Dopplick, T. G., Radiative heating of the global atmosphere: Corrigendum, *J. Atmos., Sci., 36,* 1812-1817, 1979.

DeMore, W. B., et al., Chemical kinetics and photochemical data for use in stratospheric modeling, Evaluation number 12, *JPL Publication 97-4,* Jet Propulsion Laboratory, NASA, 1997.

Fleming, E. L., S. Chandra, C. H. Jackman, D. B. Considine, and A. R. Douglass, The middle atmospheric response to short and long term solar UV variations: analysis of observations and 2D model results, *J. Atmos. Terr. Phys., 57,* 333-365, 1995.

Fleming, E. L., C. H. Jackman, R. S. Stolarski, and D. B. Considine, Simulation of stratospheric tracers using an improved empirically-based two-dimensional model transport formulation, *J. Geophys. Res.,* 104, 23,911-23,934, 1999.

Garcia, R. R., Parameterization of planetary wave breaking in the middle atmosphere, *J. Atmos. Sci., 48,* 1405-1419. 1991.

Garcia, R. R., and S. Solomon, A numerical model of the zonally averaged dynamical and chemical structure of the middle atmosphere, *J. Geophys. Res., 88,* 1379-1400, 1983.

Hall, T. M., D. W. Waugh, K. A. Boering, and R. A. Plumb, Evaluation of transport in stratospheric models, *J. Geophys. Res., 104,* 18,815-18,839, 1999.

Intergovernmental Panel on Climate Change (IPCC), *Aviation and the Global Atmosphere,* Cambridge University Press, 1999.

Jackman, C. H., A. R. Douglass, K. F. Brueske, and S. A. Klein, The influence of dynamics on two-dimensional model results: Simulations of ^{14}C and stratospheric aircraft NO_x injections, *J. Geophys. Res*, *96*, 22,559-22,572, 1991.

Jackman, C. H., E. L. Fleming, S. Chandra, D. B. Considine, and J. E. Rosenfield, Past, present, and future modeled ozone trends with comparisons to observed trends, *J. Geophys. Res.*, *101*, 28,753- 28,767, 1996.

Kalnay et al., The NCEP/NCAR 40-year reanalysis project, *Bull. Am. Meteorol. Soc.*, *77*, 437-471, 1996

Kawa, S. R., et al., Assessment of the effects of high-speed aircraft in the stratosphere: 1998, *NASA/TP-1999-209237*, 1999.

Kinnison D. E., H. S. Johnston, and D. J. Wuebbles, Model Study of Atmospheric Transport Using Carbon-14 and Strontium-90 as Inert Tracers, *J. Geophys. Res.*, *99*, 20647-20-664, 1994.

Kinnison, D. E., K. E. Grant, P. S. Connell, D. A. Rotman, and D. J. Wuebbles, The chemical and radiative effects of the Mount Pinatubo eruption, *J. Geophys. Res.*, *99*, 25,705-25,731, 1994.

Kinnison, D. E., et al., The Global Modeling Initiative assessment model: Application to high-speed civil transport perturbation, it J. Geophys. Res., 106, 1693-1711, 2001.

Ko, M. K. W., K. K. Tung, D. K. Weisenstein, and N. D. Sze, A zonal mean model of stratospheric tracer transport in isentropic coordinates: Numerical simulations for nitrous oxide and nitric acid, *J. Geophys. Res.*, *90*, 2313-2329, 1985.

Li, L., T. R. Nathan, and D. J. Wuebbles, Topographically forced planetary wave breaking in the stratosphere, *Geophys. Res. Lett.*, *22*, 2953-2956, 1995.

Lin, S. J., and R. B. Rood, Multidimensional flux-form semi-Lagrangian transport schemes, *Mon. Weather Rev., 124,*, 2046-2070, 1996.

Minschwaner, K., G. P. Anderson, L. A. Hall, and K. Yoshino, Polynomial coefficients for calculating O_2 Schumann-Runge cross sections at 0.5 cm^{-1} resolution, *J. Geophys. Res., 97,* 10103-10108, 1992.

Newell, R. E., J. W. Kidson, D. G. Vincent, and G. J. Boer, *The General Circulations of the Tropical Atmosphere, vol. 2,* chap. 7, MIT Press, Cambridge, Mass., 1974.

Oort, A.H., Global atmospheric circulation statistics, 1958-1983, *NOAA Professional Paper 14,* 1983.

Park, J. H., M. K. W. Ko, C. H. Jackman, R. A. Plumb, J. A. Kaye, and K. H. Sage, Models and Measurements Intercomparison II, *NASA/TM-1999-209554,* 1999.

Pitari, G., Contribution to the ozone trend of heterogeneous reactions of $ClONO_2$ on the sulfate aerosol layer, *Geophys. Res. Lett., 20,* 2663-2666, 1993.

Poole, L. R., and M. C. Pitts, Polar stratospheric cloud climatology based on Stratospheric Aerosol Measurement II observation from 1978 to 1989, *J. Geophys. Res., 99,* 13,083-13,089, 1994.

Prather, M. J., "I. GISS Photochemical Model", in The atmospheric effects of stratospheric aircraft: Report of the 1992 Models and Measurements Workshop, Prather, M. J., and E. E. Remsberg, eds., NASA Ref. Pub. 1292, 1993.

Prather, M. J., and E. E. Remsberg, eds., The atmospheric effects of stratospheric aircraft: Report of the 1992 Models and Measurements Workshop, NASA Ref. Pub. 1292, 1993.

Randel, W. J., and R. R. Garcia, Application of a planetary wave breaking parameterization to stratospheric circulation statistics, *J. Atmos. Sci., 51,* 1157-1168, 1994

Rosenfield, J. E., P. A. Newman, and M. R. Schoeberl, Computations of diabatic descent in the stratospheric polar vortex, *J. Geophys. Res., 99,* 16,677-16,689, 1994.

Rossow, W.B., and R.A. Schiffer, Advances in Understanding Clouds from ISCCP, *Bull. Am. Meteorol. Soc., 80,* 2261-2287, 1999.

Rotman, D. A., et al., The Global Modeling Initiative Assessment Model: Model description, integration and testing of the transport shell, *J. Geophys. Res., 106,* 1669-1691, 2001.

Sander, S. P., et al., Chemical kinetics and photochemical data for use in stratospheric modeling, Supplement to evaluation 12: Update of key reactions, Evaluation Number 13 *JPL Publication 00-3* Jet Propulsion Laboratory, NASA, 2000.

Shia, R-L, M. K. W. Ko, D. K. Weisenstein, C. Scott, and J. Rodriguez, Transport between the tropical and mid-latitude lower stratosphere: Implication for ozone response to HSCT emissions, *J. Geophys. Res.,* 103, 25,435-25,446, 1998.

Smolarkiewicz, P. K., A simple positive definite advection scheme with small implicit diffusion, *Mon. Weather Rev., 111,* 479-487, 1984.

Stolarski, R. S., et al., 1995 scientific assessment of the atmospheric effects of stratospheric aircraft, *NASA Ref. Pub 1381,* 1995.

Weisenstein, D. K., M. K. W. Ko, I. G . Dyominov, G. Pitari, L. Ricciardulli, G. Visconti, and S. Bekki, The effect of sulfur emissions from HSCT aircraft: A 2-D model intercomparison, *J. Geophys. Res., 103,* 1527-1547, 1998.

WMO, Scientific Assessment of Ozone Depletion: 1991, *World Meteorological Organization Global Ozone Research and Monitoring Project Report No. 25,* Geneva, 1992.

Figure 1. LLNL model values of K_{yy} (in 10^{10} cm^2/s) (panels a and b) and vertical velocity (in mm/s) (panels c and d) for June (panels a and c) and December (panels b and d).

Figure 2. GSFC model values of K_{yy} (in 10^{10} cm^2/s) (panels a and b) and vertical velocity (in mm/s) (panels c and d) for June (panels a and c) and December (panels b and d).

Figure 3. AER model values of K_{yy} (in 10^{10} cm^2/s) (panels a and b) and vertical velocity (in mm/s) (panels c and d) for June (panels a and c) and December (panels b and d).

Figure 4. Calculated mixing ratio (ppbv) for June of an inert tracer with source similar to HSCT aircraft emission of NO_y and tropospheric sink. Panel (a) shows AER model results, panel (b) AER/GSFC results, panel (c) AER/LLNL results, panel (d) GSFC results, and panel (e) LLNL results.

Figure 5. October mixing ratios of (a) NO_y in ppbv, (b) H_2O in ppmv, (c) Cl_y in ppbv, (d) O_3 in ppmv, and (e) O_3 column in dobson units as calculated by the AER model for steady-state 2015 conditions.

Figure 6. October NO_y mixing ratio differences (ppbv) between the GSFC and AER models in a 2015 background atmosphere with subsonic aircraft. Panel (a) shows the difference between the GSFC and AER models with PSC chemistry included, panel (b) the difference between the AER/GSFC and AER models, and panel (c) the difference between the GSFC and AER/GSFC models. Panel (d) shows the difference between the GSFC and AER/GSFC models without PSC chemistry.

Figure 7. October NO_y mixing ratio differences (ppbv) between the LLNL and AER models in a 2015 background atmosphere with subsonic aircraft. Panel (a) shows the difference between the LLNL and AER models with PSC chemistry included, panel (b) the difference between the AER/LLNL and AER models, and panel (c) the difference between the LLNL and AER/LLNL models. Panel (d) shows the difference between the LLNL and AER/LLNL models without PSC chemistry.

Figure 8. October H_2O mixing ratio differences (ppmv) between the GSFC and AER models in a 2015 background atmosphere with subsonic aircraft. Panel (a) shows the difference between the GSFC and AER models with PSC chemistry included, panel (b) the difference between the AER/GSFC and AER models, and panel (c) the difference between the GSFC and AER/GSFC models. Panel (d) shows the difference between the GSFC and AER/GSFC models without PSC chemistry.

Figure 9. October H_2O mixing ratio differences (ppmv) between the LLNL and AER models in a 2015 background atmosphere with subsonic aircraft. Panel (a) shows the difference between the LLNL and AER models with PSC chemistry included, panel (b) the difference between the AER/LLNL and AER models, and panel (c) the difference between the LLNL and AER/LLNL models. Panel (d) shows the difference between the LLNL and AER/LLNL models without PSC chemistry.

Figure 10. October Cl_y mixing ratio differences (ppbv) between the GSFC and AER models in a 2015 background atmosphere with subsonic aircraft. Panel (a) shows the difference between the GSFC and AER models with PSC chemistry included, panel (b) the difference between the AER/GSFC and AER models, and panel (c) the difference between the GSFC and AER/GSFC models. Panel (d) shows the difference between the GSFC and AER/GSFC models without PSC chemistry.

Figure 11. October Cl_y mixing ratio differences (ppbv) between the LLNL and AER models in a 2015 background atmosphere with subsonic aircraft. Panel (a) shows the difference between the LLNL and AER models with PSC chemistry included, panel (b) the difference between the AER/LLNL and AER models, and panel (c) the difference between the LLNL and AER/LLNL models. Panel (d) shows the difference between the LLNL and AER/LLNL models without PSC chemistry.

Figure 12. October O_3 mixing ratio differences (ppmv) between the GSFC and AER models in a 2015 background atmosphere with subsonic aircraft. Panel (a) shows the difference between the GSFC and AER models with PSC chemistry included, panel (b) the difference between the AER/GSFC and AER models, and panel (c) the difference between the GSFC and AER/GSFC models. Panel (d) shows the difference between the GSFC and AER/GSFC models without PSC chemistry.

Figure 13. October O_3 mixing ratio differences (ppmv) between the LLNL and AER models in a 2015 background atmosphere with subsonic aircraft. Panel (a) shows the difference between the LLNL and AER models with PSC chemistry included, panel (b) the difference between the AER/LLNL and AER models, and panel (c) the difference between the LLNL and AER/LLNL models. Panel (d) shows the difference between the LLNL and AER/LLNL models without PSC chemistry.

Figure 14. O_3 column differences (Dobson units) between the GSFC and AER models in a 2015 background atmosphere with subsonic aircraft. Panel (a) shows the difference between the GSFC and AER models with PSC chemistry included, panel (b) the difference between the AER/GSFC and AER models, and panel (c) the difference between the GSFC and AER/GSFC models. Panel (d) shows the difference between the GSFC and AER/GSFC models without PSC chemistry.

Figure 15. O_3 column differences (Dobson units) between the LLNL and AER models in a 2015 background atmosphere with subsonic aircraft. Panel (a) shows the difference between the LLNL and AER models with PSC chemistry included, panel (b) the difference between the AER/LLNL and AER models, and panel (c) the difference between the LLNL and AER/LLNL models. Panel (d) shows the difference between the LLNL and AER/LLNL models without PSC chemistry.

Figure 16. Calculated perturbation in H_2O (ppmv) for October due to emission from HSCT aircraft in 2015 relative to an atmosphere with only subsonic aircraft. Panel (a) shows AER model results, panel (b) AER/GSFC results, panel (c) AER/LLNL results, panel (d) GSFC results, and panel (e) LLNL results, all without PSC chemistry.

Figure 17. Calculated perturbation in NO_y (ppbv) for October due to emission from HSCT aircraft in 2015 relative to an atmosphere with only subsonic aircraft. Panel (a) shows AER model results, panel (b) AER/GSFC results, panel (c) AER/LLNL results, panel (d) GSFC results, and panel (e) LLNL results, all without PSC chemistry.

Figure 18. Calculated perturbation in O_3 (%) for October due to emission from HSCT aircraft in 2015 relative to an atmosphere with only subsonic aircraft. Panel (a) shows AER model results, panel (b) AER/GSFC results, panel (c) AER/LLNL results, panel (d) GSFC results, and panel (e) LLNL results, all without PSC chemistry.

Figure 19. Calculated perturbation in O_3 column (%) due to emission from HSCT aircraft in 2015 relative to an atmosphere with only subsonic aircraft. Panel (a) shows AER model results, panel (b) AER/GSFC results, panel (c) AER/LLNL results, panel (d) GSFC results, and panel (e) LLNL results, all without PSC chemistry.

Figure 20. Calculated perturbation in O_3 (%) for October due to emission from HSCT aircraft in 2015 relative to an atmosphere with only subsonic aircraft. Panel (a) shows AER model results, panel (b) AER/GSFC results, panel (c) AER/LLNL results, panel (d) GSFC results, and panel (e) LLNL results, all with PSC chemistry.

Figure 21. Calculated perturbation in O_3 column (%) due to emission from HSCT aircraft in 2015 relative to an atmosphere with only subsonic aircraft. Panel (a) shows AER model results, panel (b) AER/GSFC results, panel (c) AER/LLNL results, panel (d) GSFC results, and panel (e) LLNL results, all with PSC chemistry.

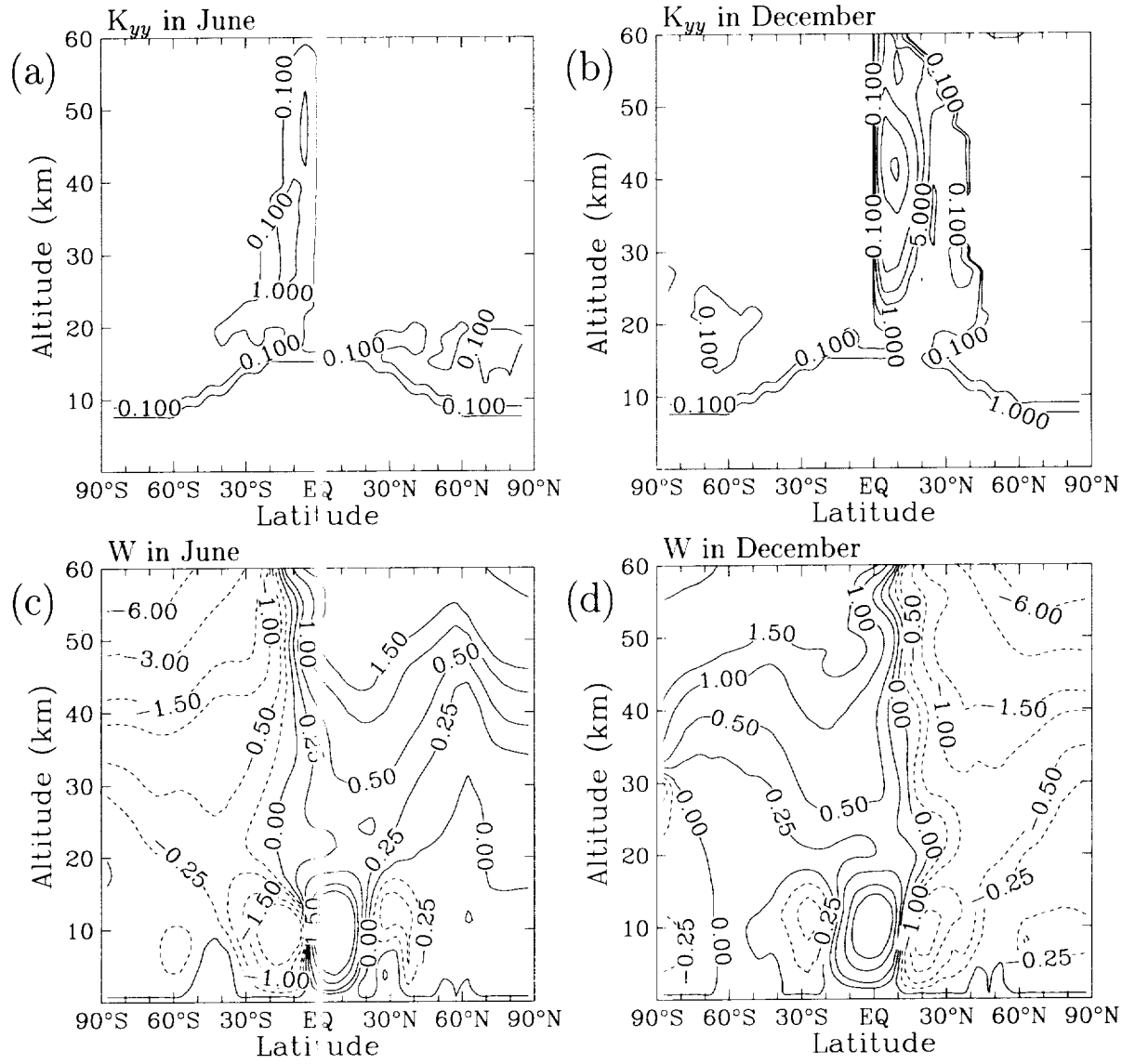

Figure 1. LLNL model values of K_{yy} (in 10^{10} cm^2/s) (panels a and b) and vertical velocity (in mm/s) (panels c and d) for June (panels a and c) and December (panels b and d).

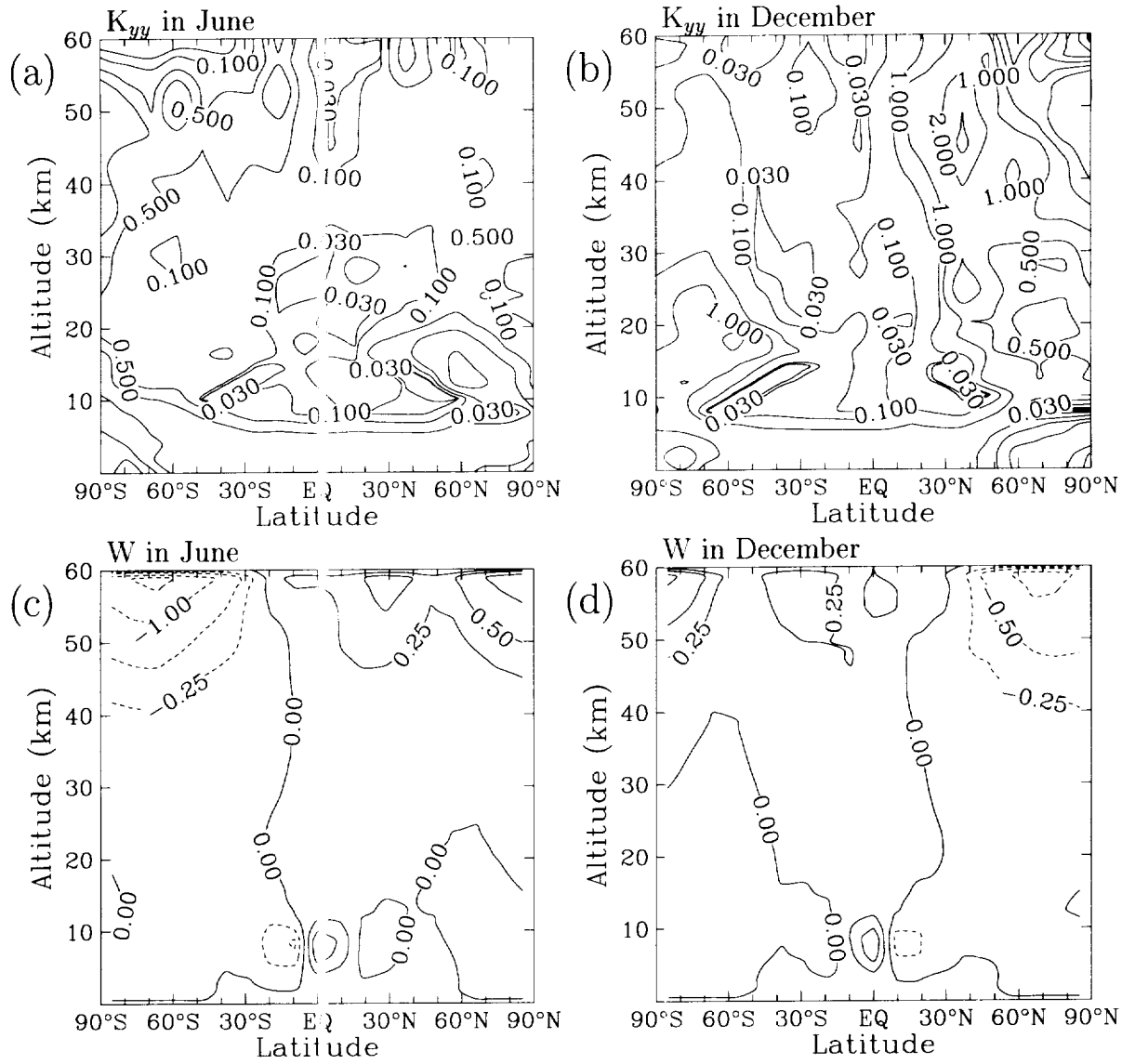

Figure 2. GSFC model values of K_{yy} (in 10^{10} cm^2/s) (panels a and b) and vertical velocity (in mm/s) (panels c and d) for June (panels a and c) and December (panels b and d).

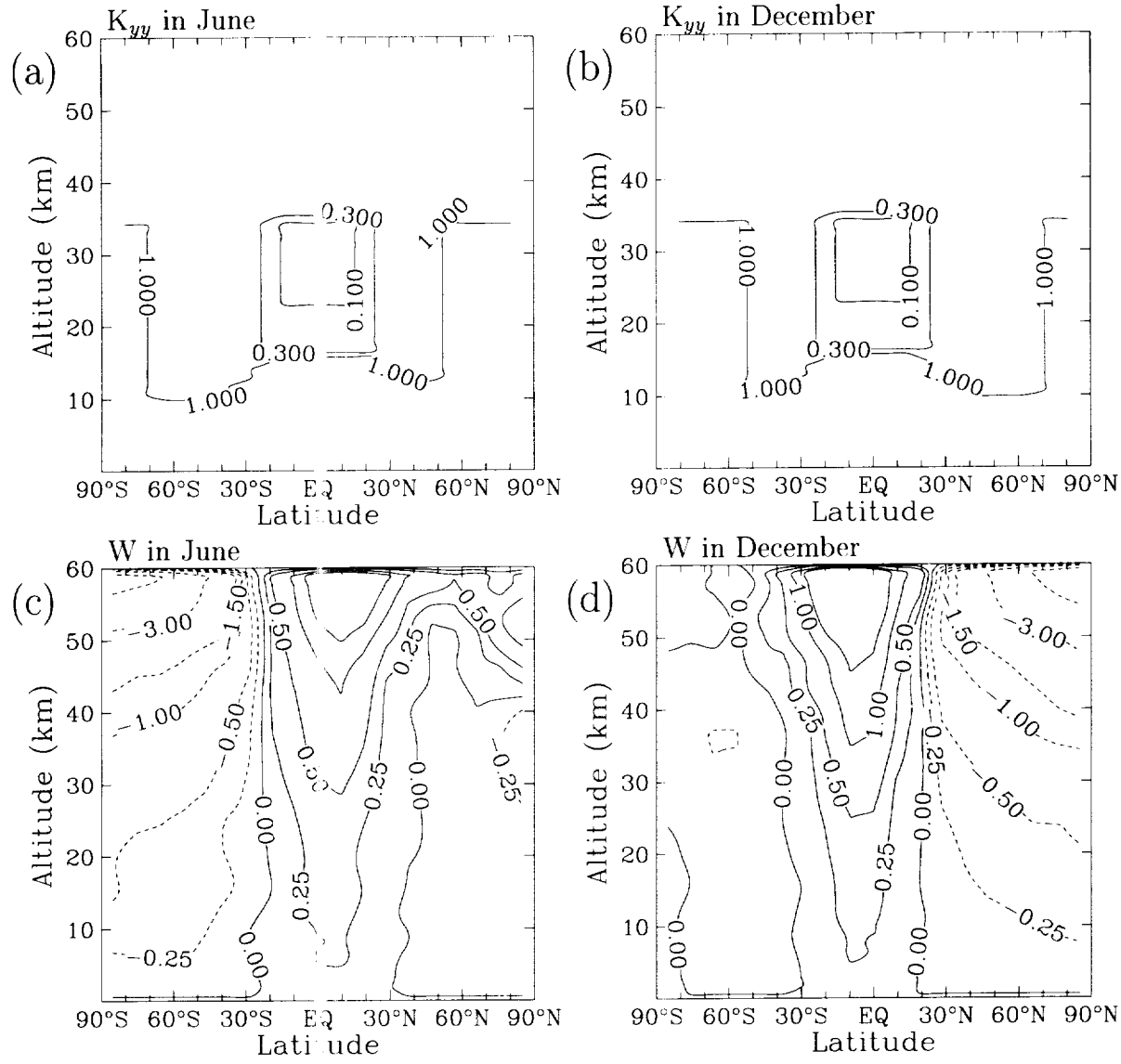

Figure 3. AER model values of K_{yy} (in 10^{10} cm^2/s) (panels a and b) and vertical velocity (in mm/s) (panels c and d) for June (panels a and c) and December (panels b and d).

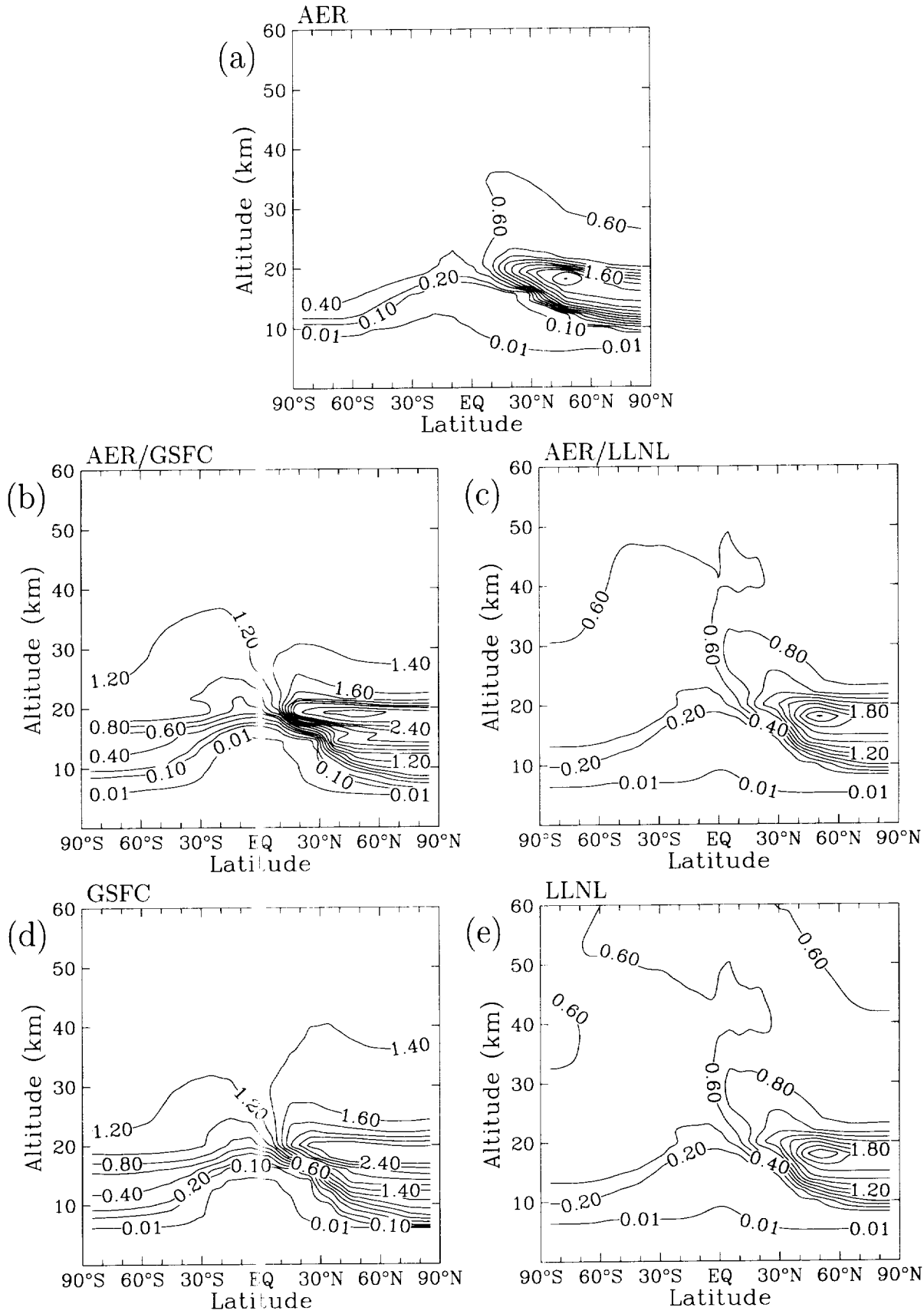

Figure 4. Calculated mixing ratio (ppbv) for June of an inert tracer with source similar to HSCT aircraft emission of NO_y and tropospheric sink. Panel (a) shows AER model results, panel (b) AER/GSFC results, panel (c) AER/LLNL results, panel (d) GSFC results, and panel (e) LLNL results. Contours are 0.01, 0.1, 0.2-2.4 by 0.2, 2.8, and 3.2.

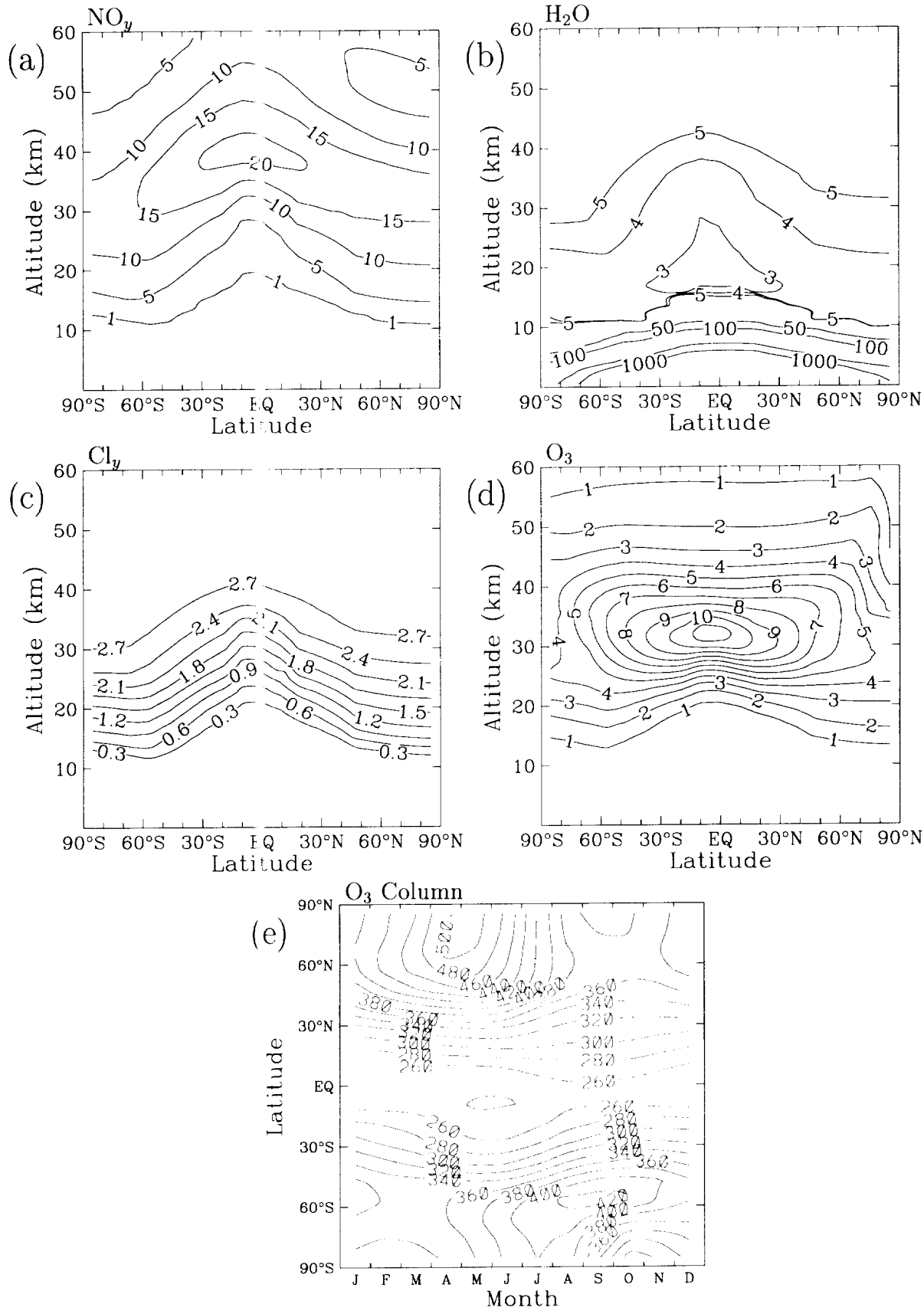

Figure 5. October mixing ratios of (a) NO_y in ppbv, (b) H_2O in ppmv, (c) Cl_y in ppbv, (d) O_3 in ppmv, and (e) O_3 column in dobson units as calculated by the AER model for steady-state 2015 conditions.

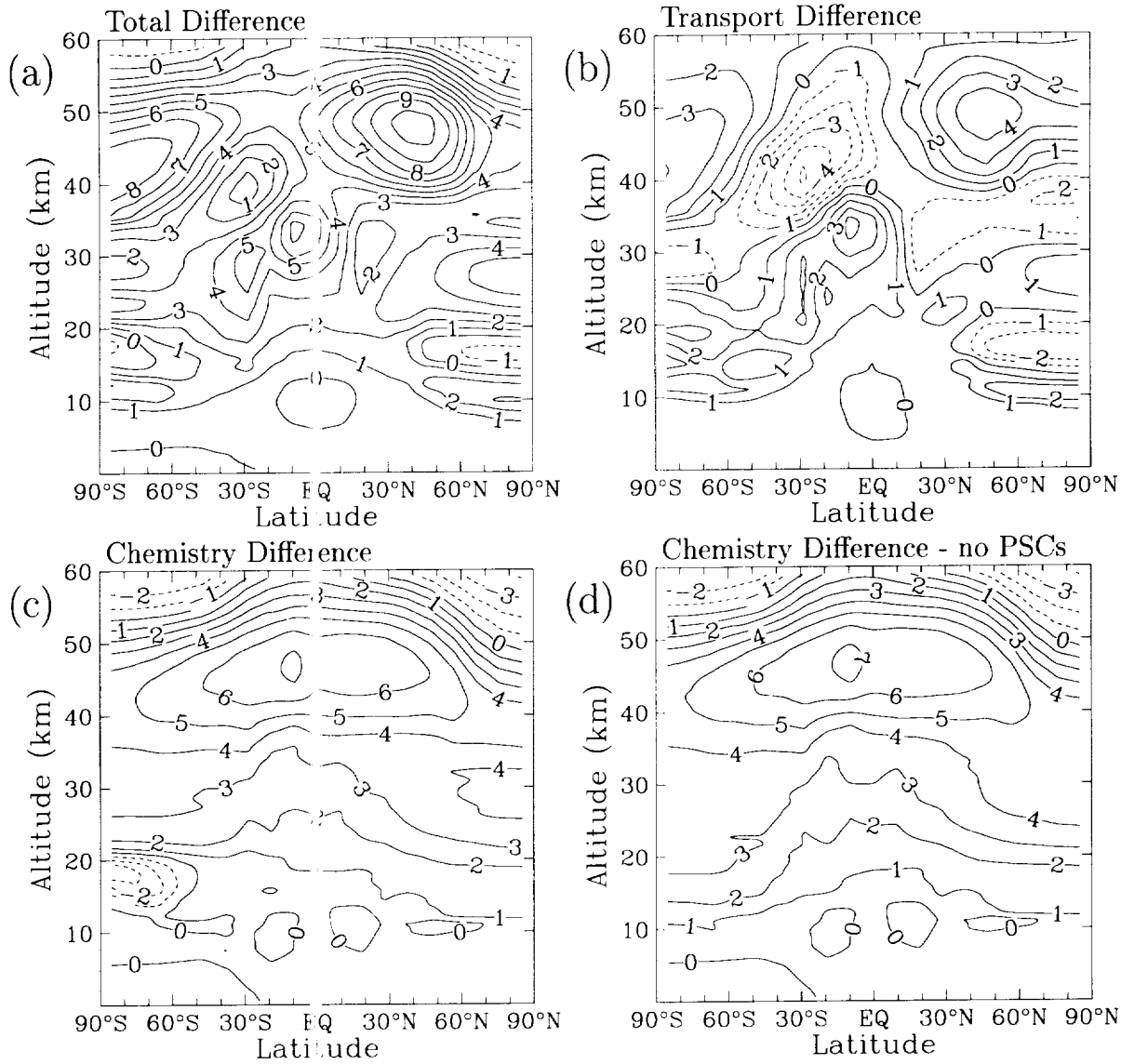

Figure 6. October NO_y mixing ratio differences (ppbv) between the GSFC and AER models in a 2015 background atmosphere with subsonic aircraft. Panel (a) shows the difference in the GSFC and AER models with PSC chemistry included, panel (b) is the AER/GSFC-AER difference, and panel (c) shows the GSFC - AER/GSFC model difference. Panel (d) is the GSFC - AER/GSFC model difference without PSC chemistry.

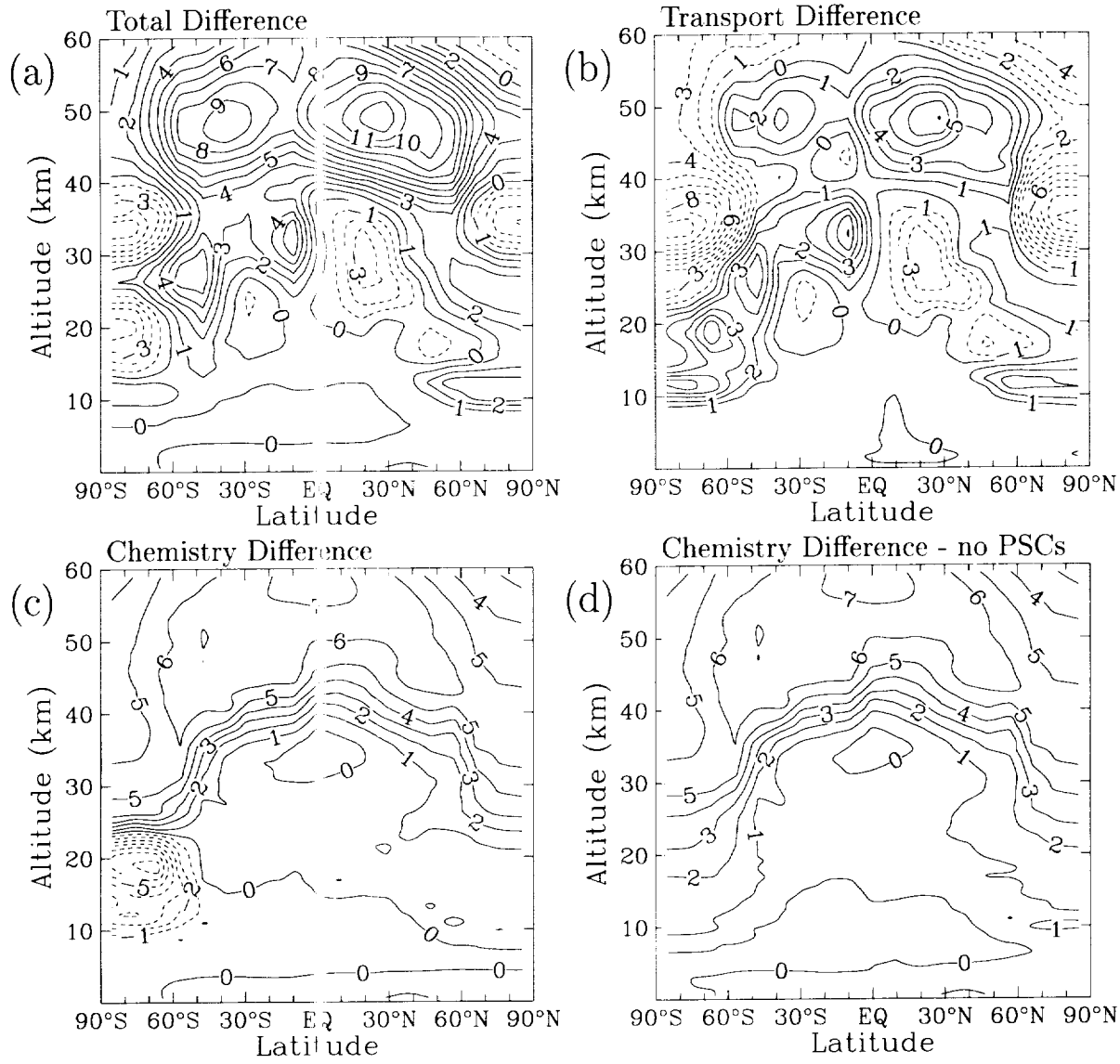

Figure 7. October NO_y mixing ratio differences (ppbv) between the LLNL and AER models in a 2015 background atmosphere with subsonic aircraft. Panel (a) shows the difference in the LLNL and AER models with PSC chemistry included, panel (b) is the AER/LLNL-AER difference, and panel (c) shows the LLNL - AER/LLNL model difference. Panel (d) is the LLNL - AER/LLNL model difference without PSC chemistry.

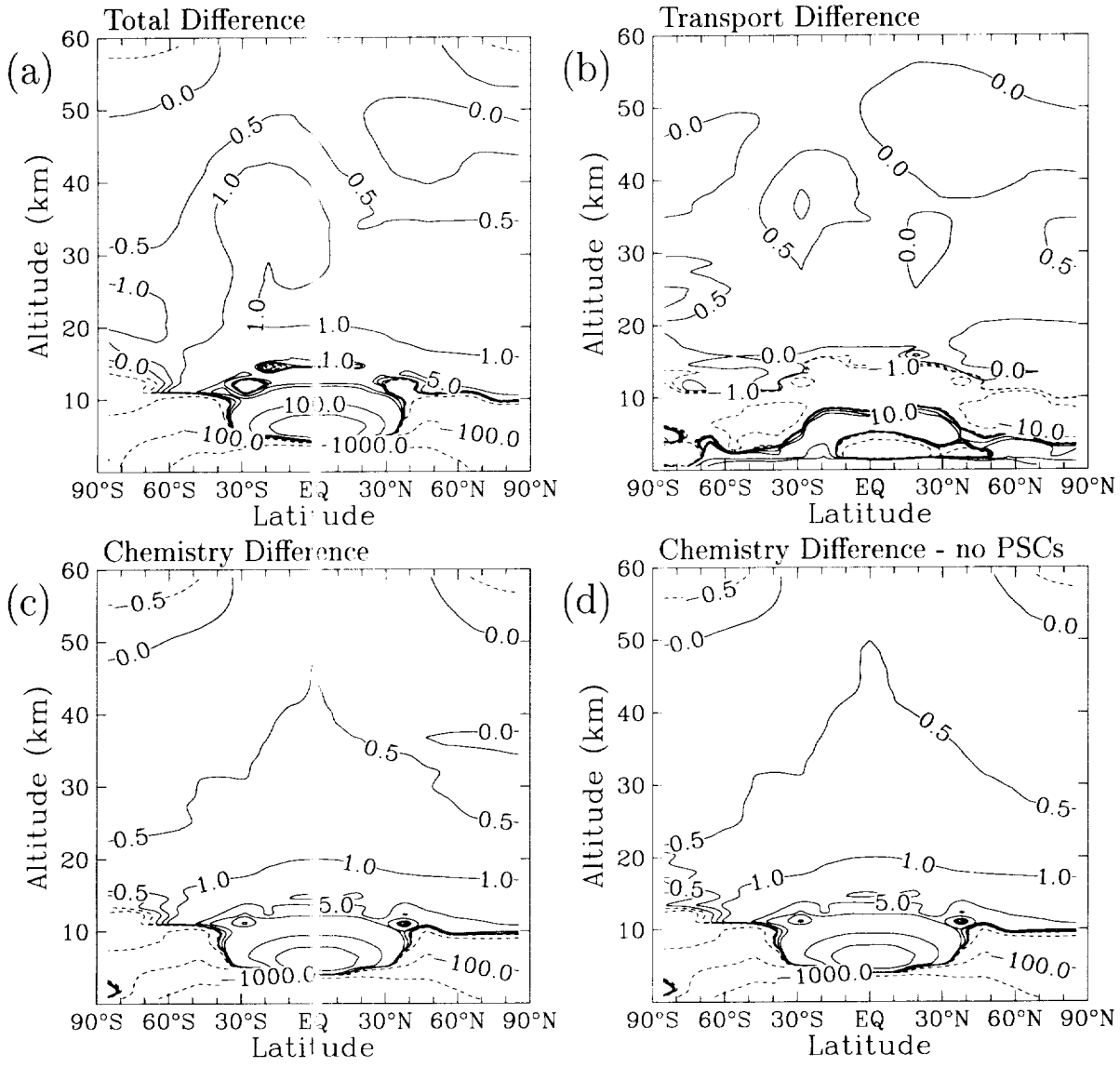

Figure 8. October H_2O mixing ratio differences (ppmv) between the GSFC and AER models in a 2015 background atmosphere with subsonic aircraft. Panel (a) shows the difference in the GSFC and AER models with PSC chemistry included, panel (b) is the AER/GSFC-AER difference, and panel (c) shows the GSFC - AER/GSFC model difference. Panel (d) is the GSFC - AER/GSFC model difference without PSC chemistry.

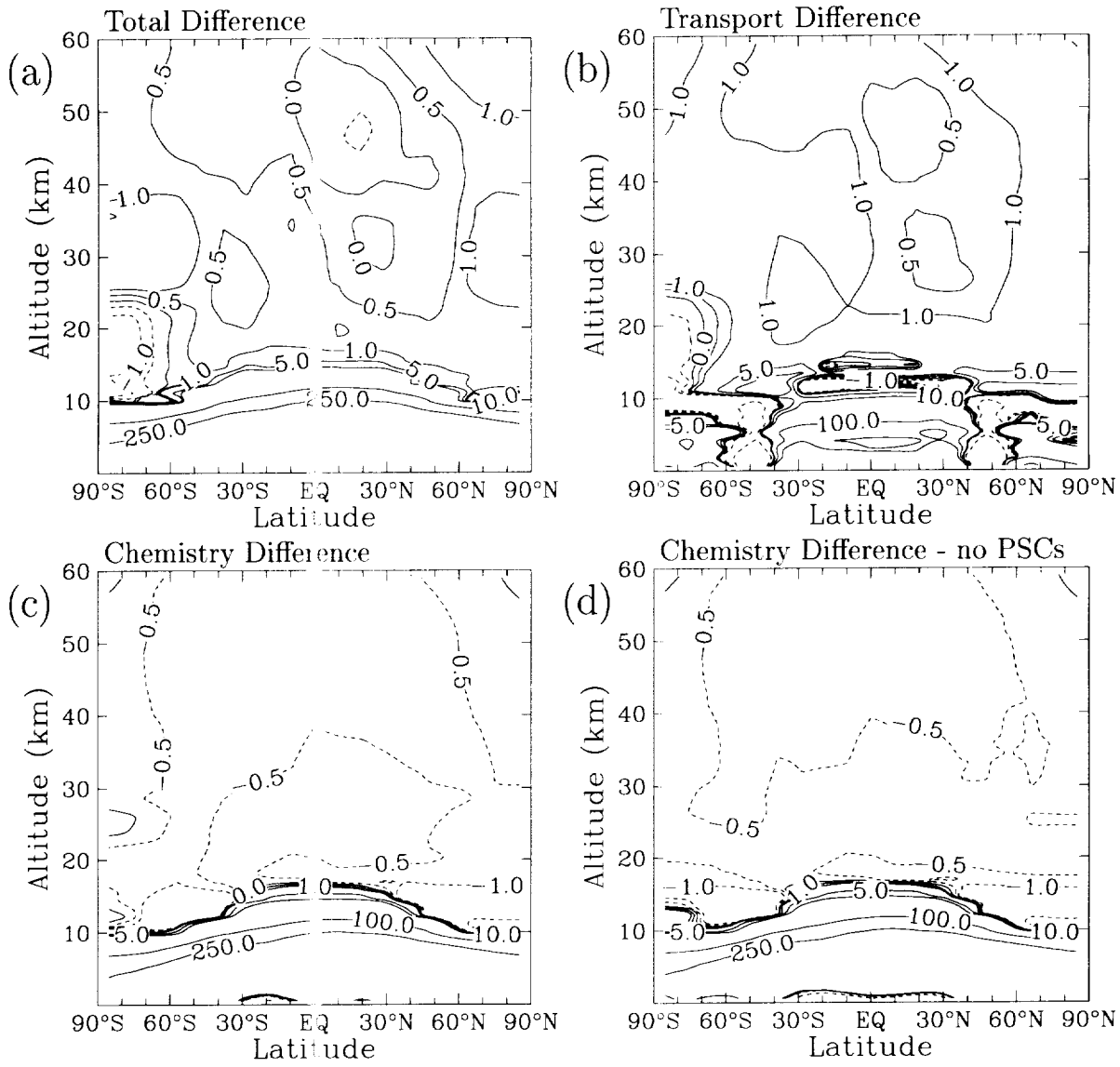

Figure 9. October H_2O mixing ratio differences (ppmv) between the LLNL and AER models in a 2015 background atmosphere with subsonic aircraft. Panel (a) shows the difference in the LLNL and AER models with PSC chemistry included, panel (b) is the AER/LLNL-AER difference, and panel (c) shows the LLNL - AER/LLNL model difference. Panel (d) is the LLNL - AER/LLNL model difference without PSC chemistry.

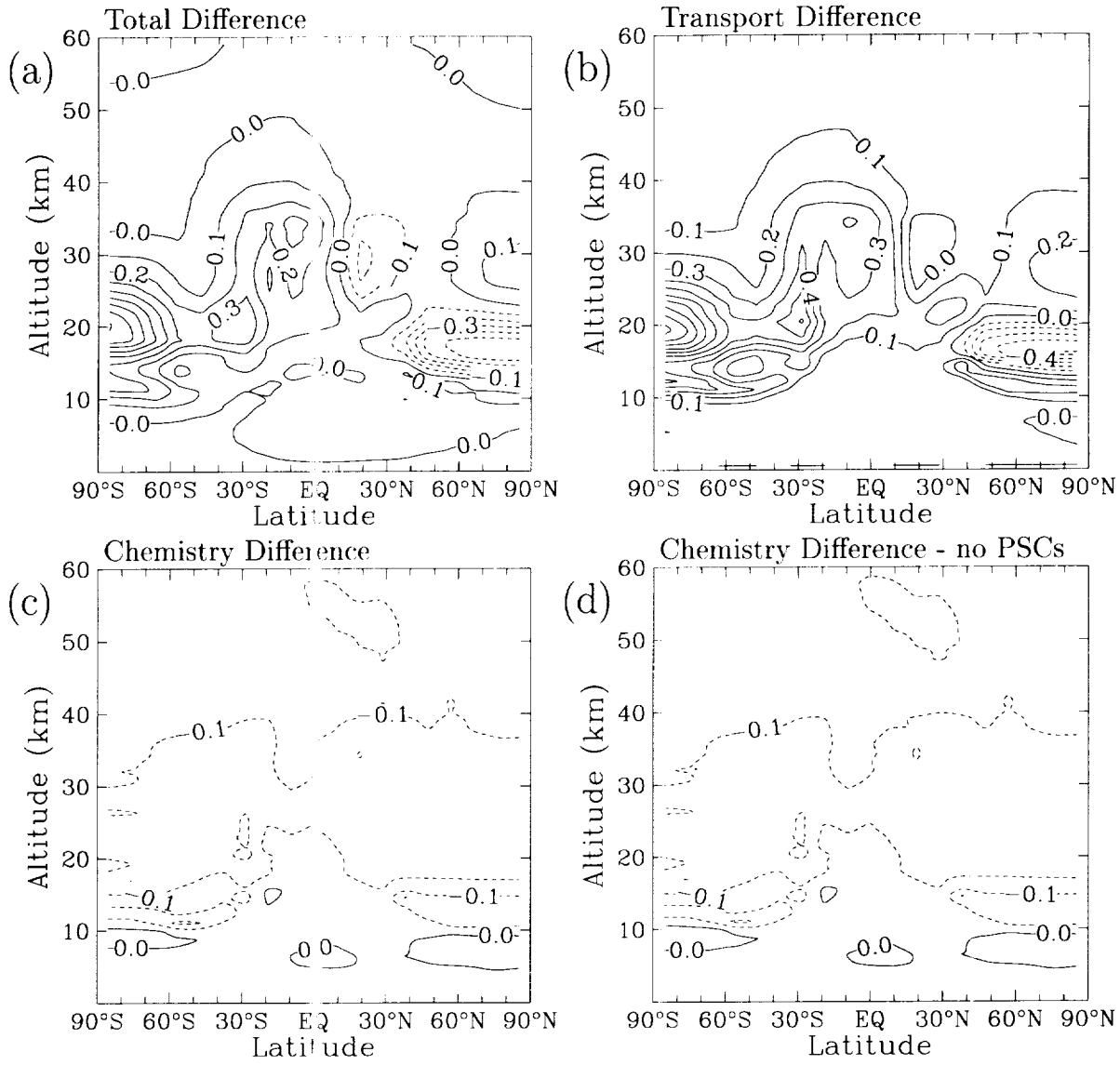

Figure 10. October Cl_y mixing ratio differences (ppbv) between the GSFC and AER models in a 2015 background atmosphere with subsonic aircraft. Panel (a) shows the difference in the GSFC and AER models with PSC chemistry included, panel (b) is the AER/GSFC-AER difference, and panel (c) shows the GSFC - AER/GSFC model difference. Panel (d) is the GSFC - AER/GSFC model difference without PSC chemistry.

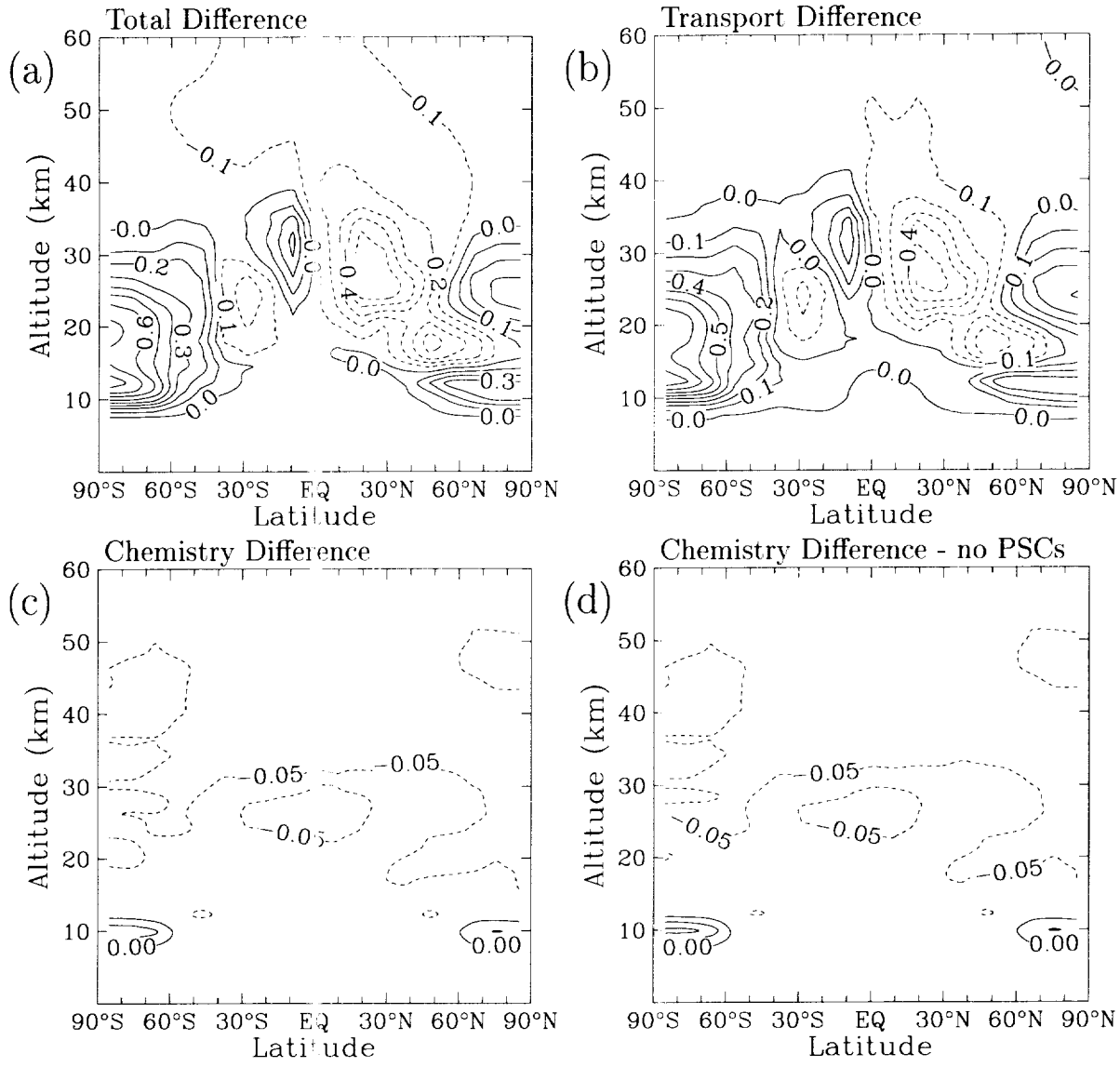

Figure 11. October Cl_y mixing ratio differences (ppbv) between the LLNL and AER models in a 2015 background atmosphere with subsonic aircraft. Panel (a) shows the difference in the LLNL and AER models with PSC chemistry included, panel (b) is the AER/LLNL-AER difference, and panel (c) shows the LLNL - AER/LLNL model difference. Panel (d) is the LLNL - AER/LLNL model difference without PSC chemistry.

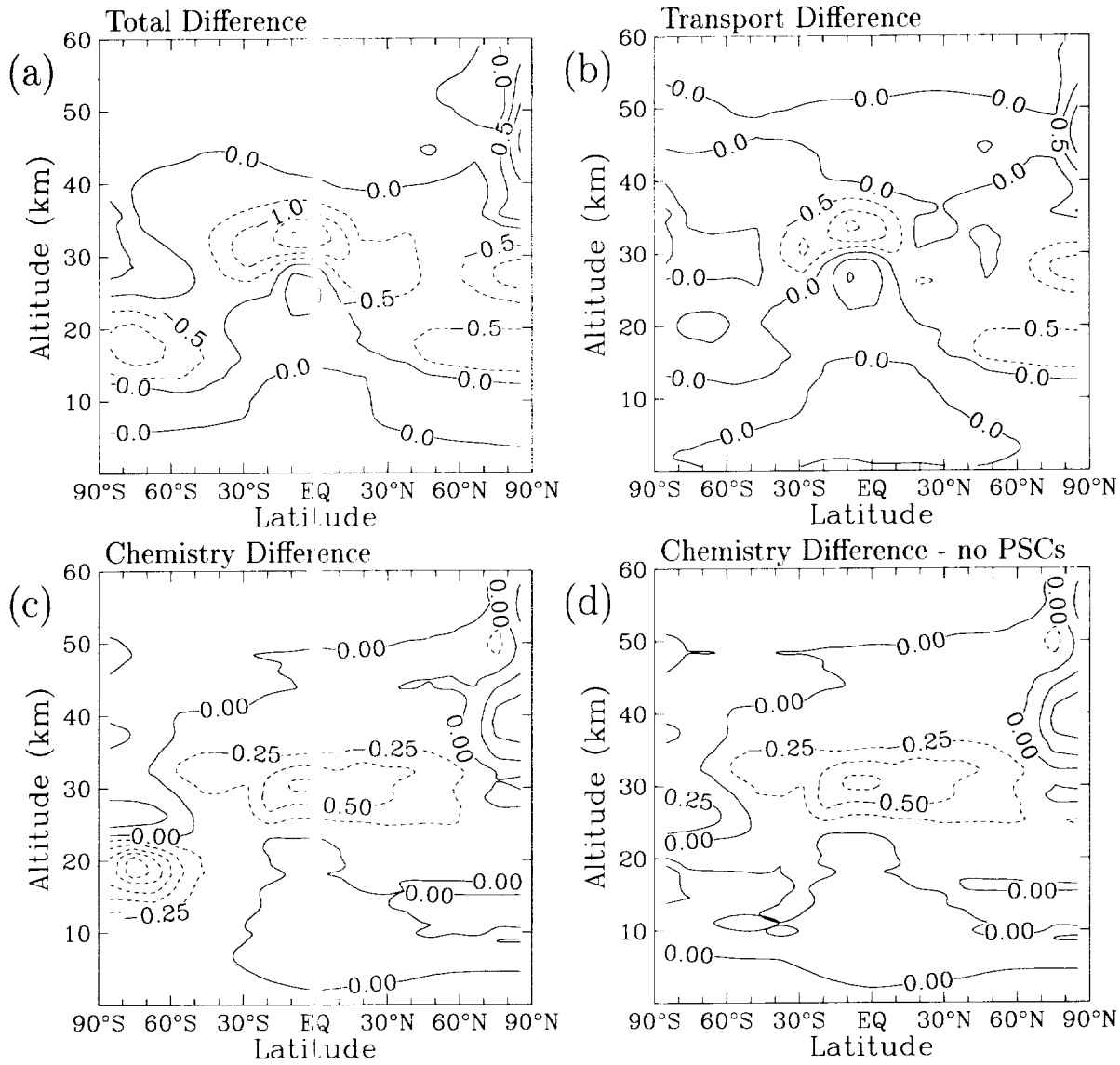

Figure 12. October O_3 mixing ratio differences (ppmv) between the GSFC and AER models in a 2015 background atmosphere with subsonic aircraft. Panel (a) shows the difference in the GSFC and AER models with PSC chemistry included, panel (b) is the AER/GSFC-AER difference, and panel (c) shows the GSFC - AER/GSFC model difference. Panel (d) is the GSFC - AER/GSFC model difference without PSC chemistry.

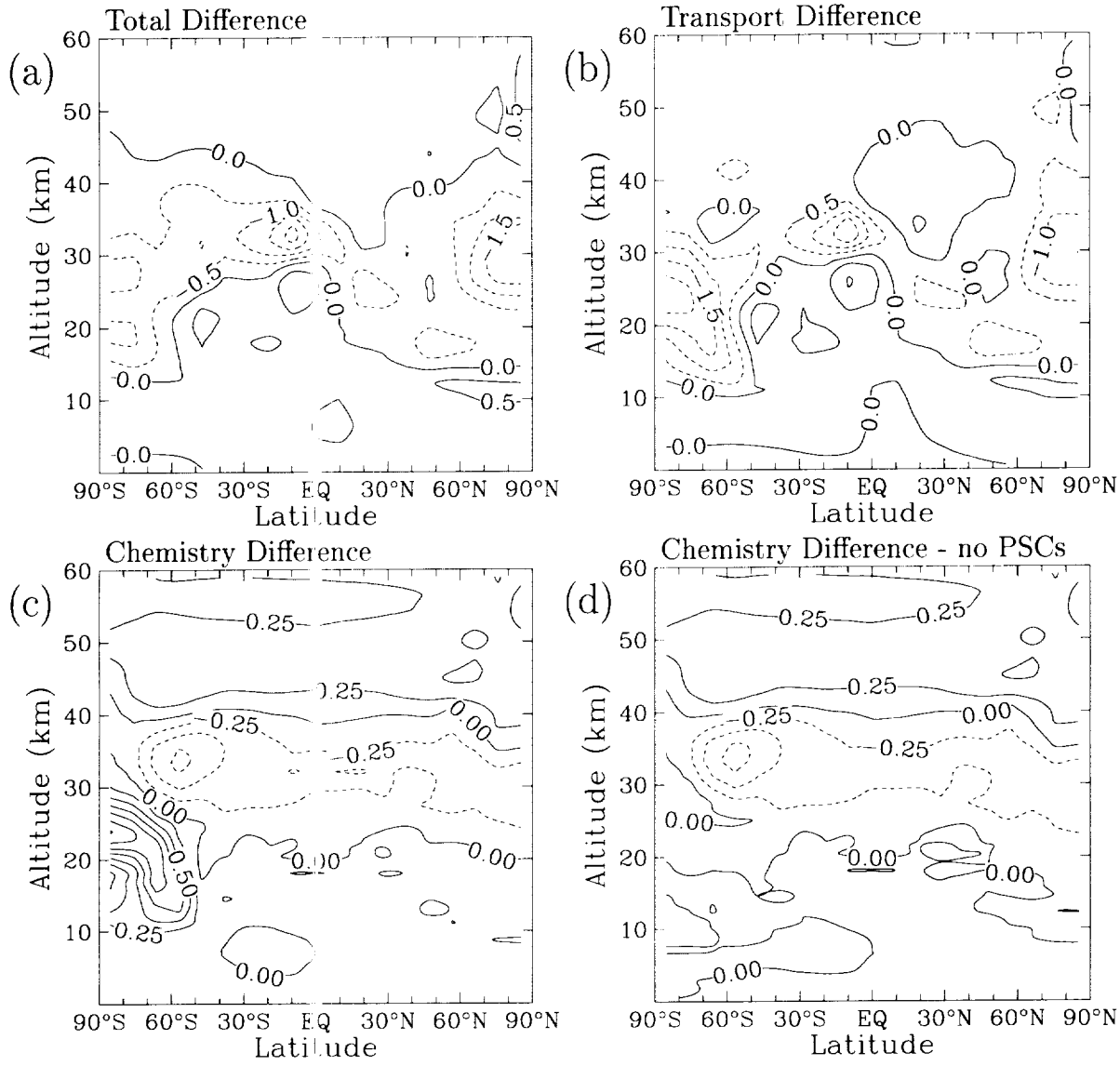

Figure 13. October O_3 mixing ratio differences (ppmv) between the LLNL and AER models in a 2015 background atmosphere with subsonic aircraft. Panel (a) shows the difference in the LLNL and AER models with PSC chemistry included, panel (b) is the AER/LLNL-AER difference, and panel (c) shows the LLNL - AER/LLNL model difference. Panel (d) is the LLNL - AER/LLNL model difference without PSC chemistry.

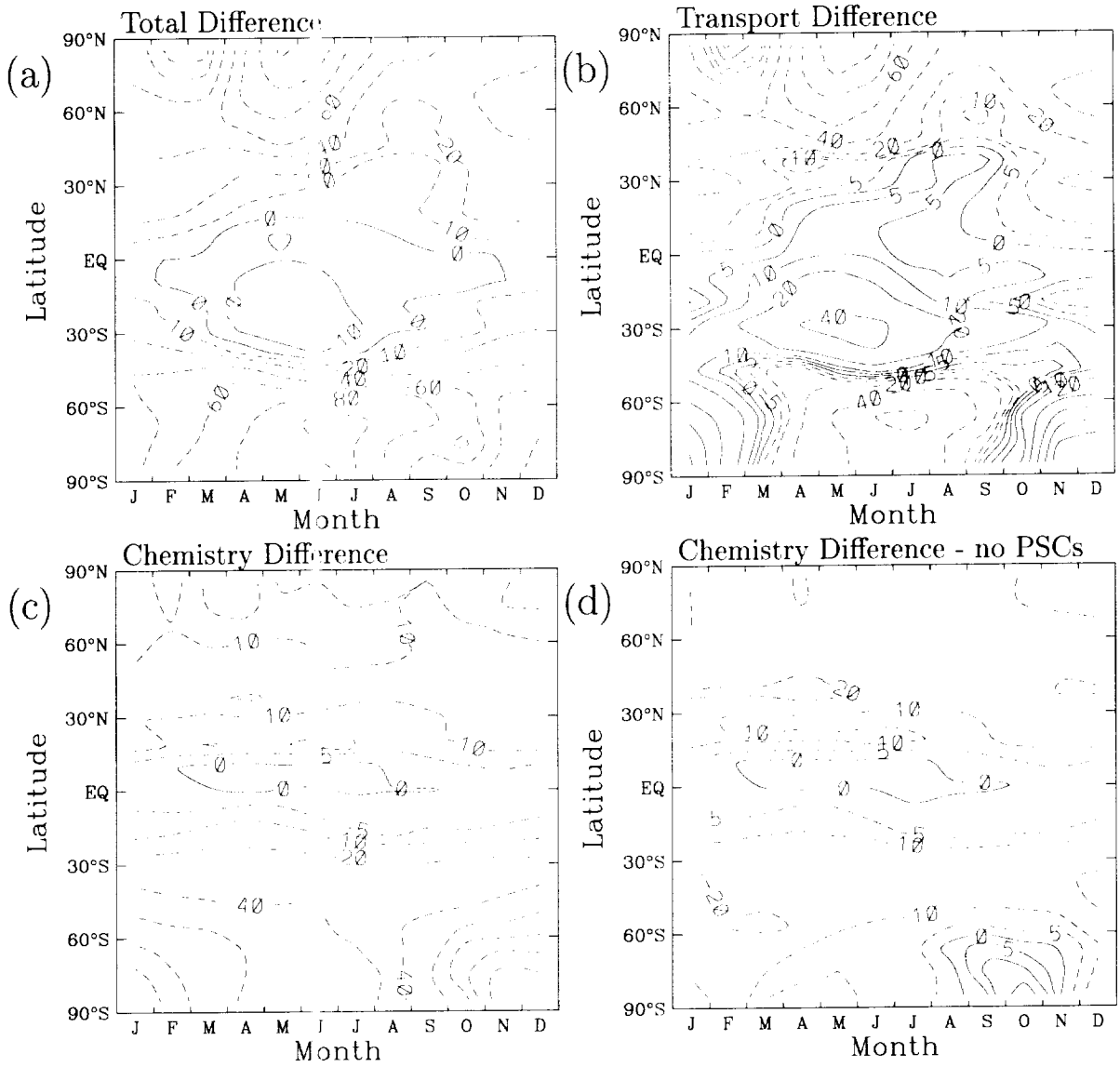

Figure 14. O_3 column differences (Dobson units) between the GSFC and AER models in a 2015 background atmosphere with subsonic aircraft. Panel (a) shows the difference between the GSFC and AER models with PSC chemistry included, panel (b) the difference between the AER/GSFC and AER models, and panel (c) the difference between the GSFC and AER/GSFC models. Panel (d) shows the difference between the GSFC and AER/GSFC models without PSC chemistry.

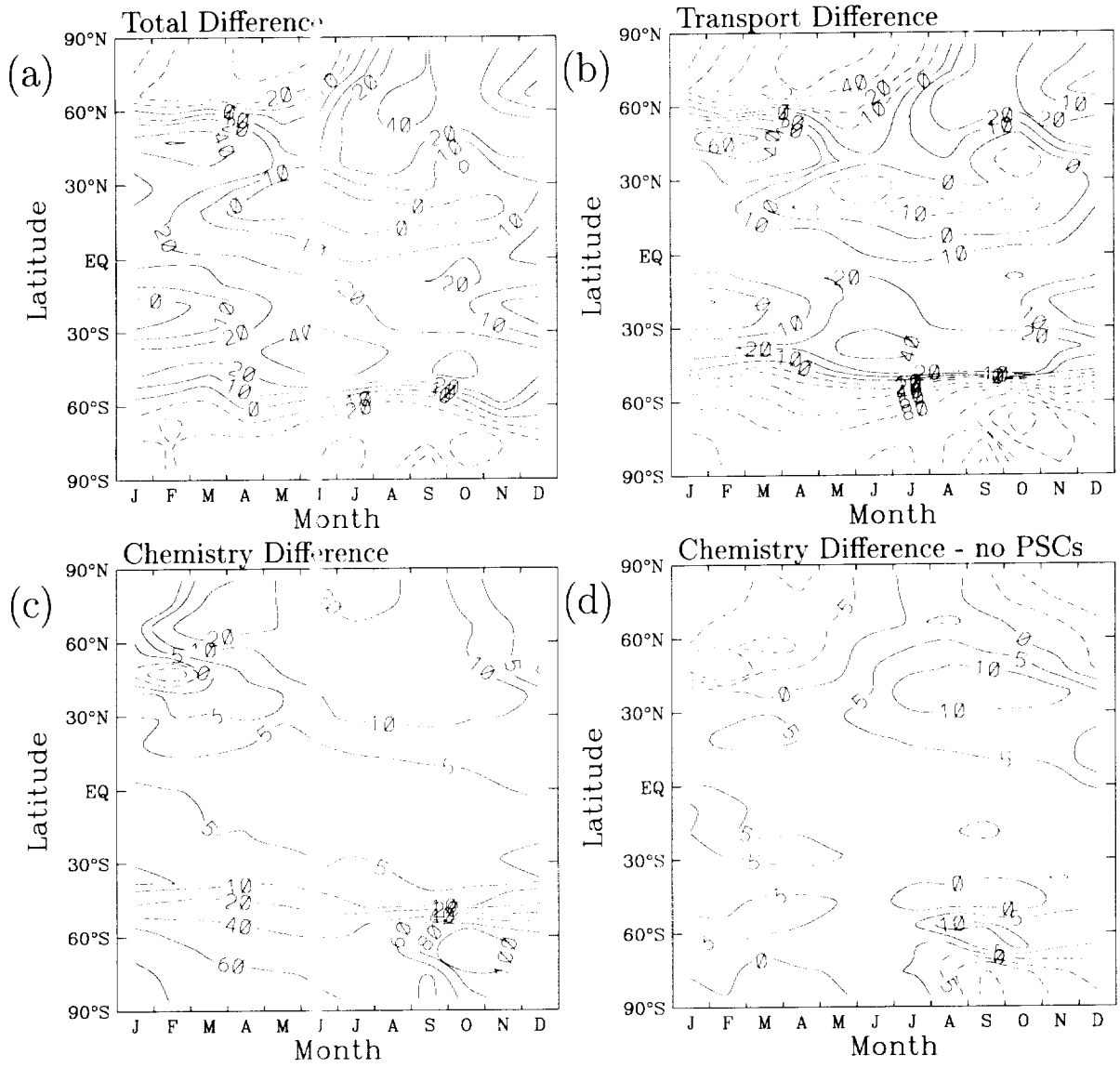

Figure 15. O_3 column differences (Dobson units) between the LLNL and AER models in a 2015 background atmosphere with subsonic aircraft. Panel (a) shows the difference between the LLNL and AER models with PSC chemistry included, panel (b) the difference between the AER/LLNL and AER models, and panel (c) the difference between the LLNL and AER/LLNL models. Panel (d) shows the difference between the LLNL and AER/LLNL models without PSC chemistry.

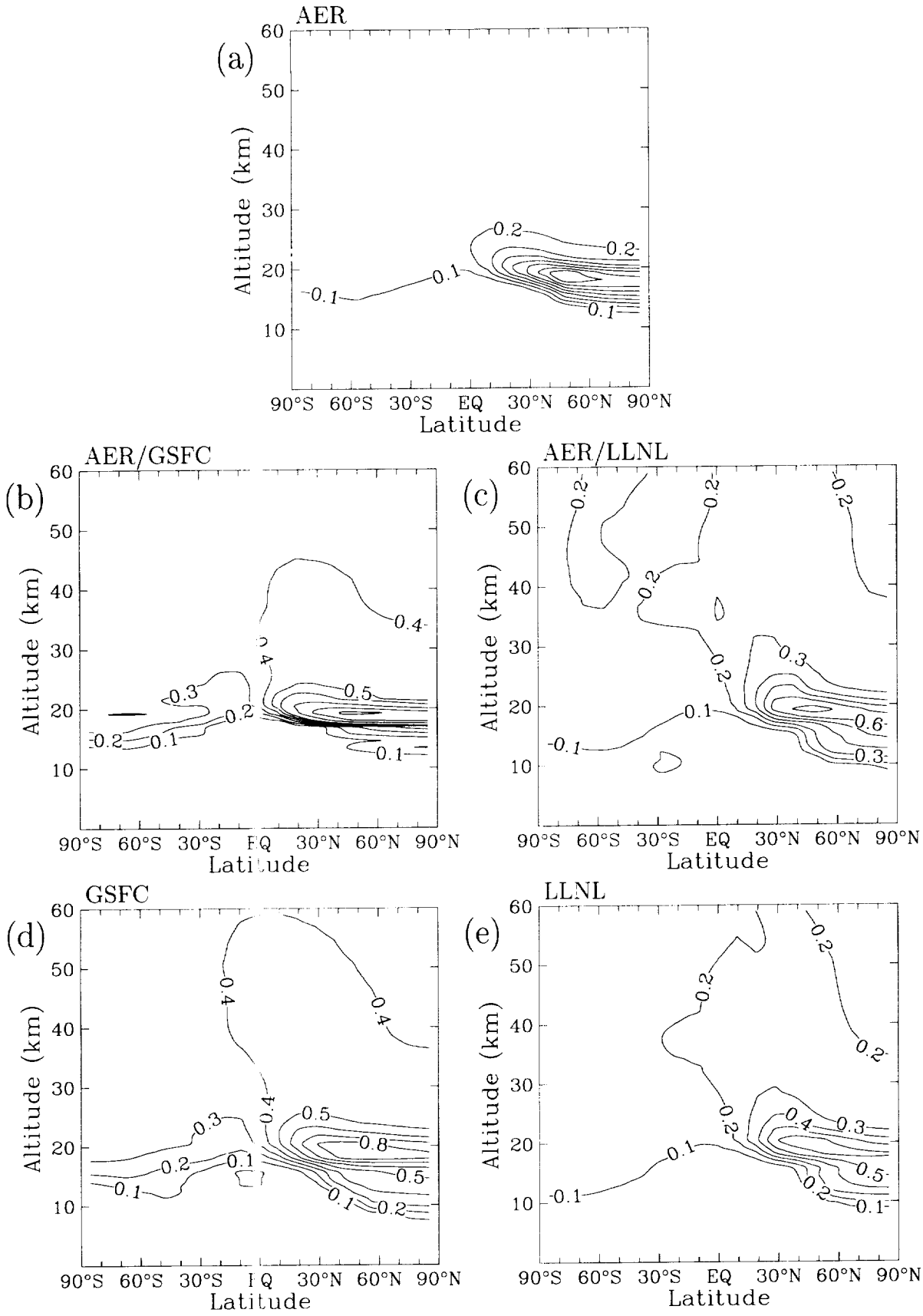

Figure 16. Calculated perturbation in H_2O (ppmv) for October due to emission from HSCT aircraft in 2015 relative to an atmosphere with only subsonic aircraft. Panel (a) shows AER model results, panel (b) AER/GSFC results, panel (c) AER/LLNL results, panel (d) GSFC results, and panel (e) LLNL results, all without PSC chemistry.

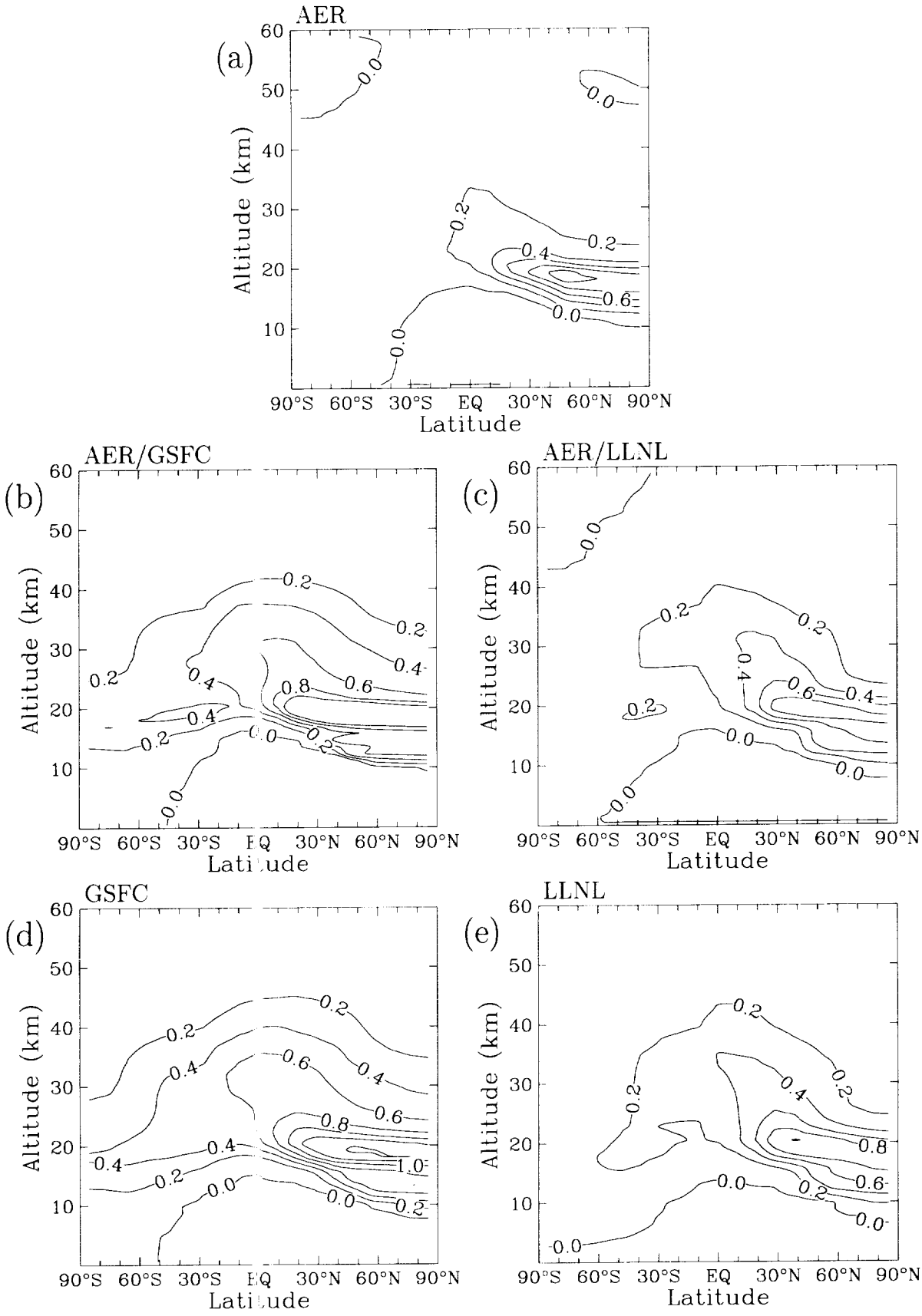

Figure 17. Calculated perturbation in NO_y (ppbv) for October due to emission from HSCT aircraft in 2015 relative to an atmosphere with only subsonic aircraft. Panel (a) shows AER model results, panel (b) AER/GSFC results, panel (c) AER/LLNL results, panel (d) GSFC results, and panel (e) LLNL results, all without PSC chemistry.

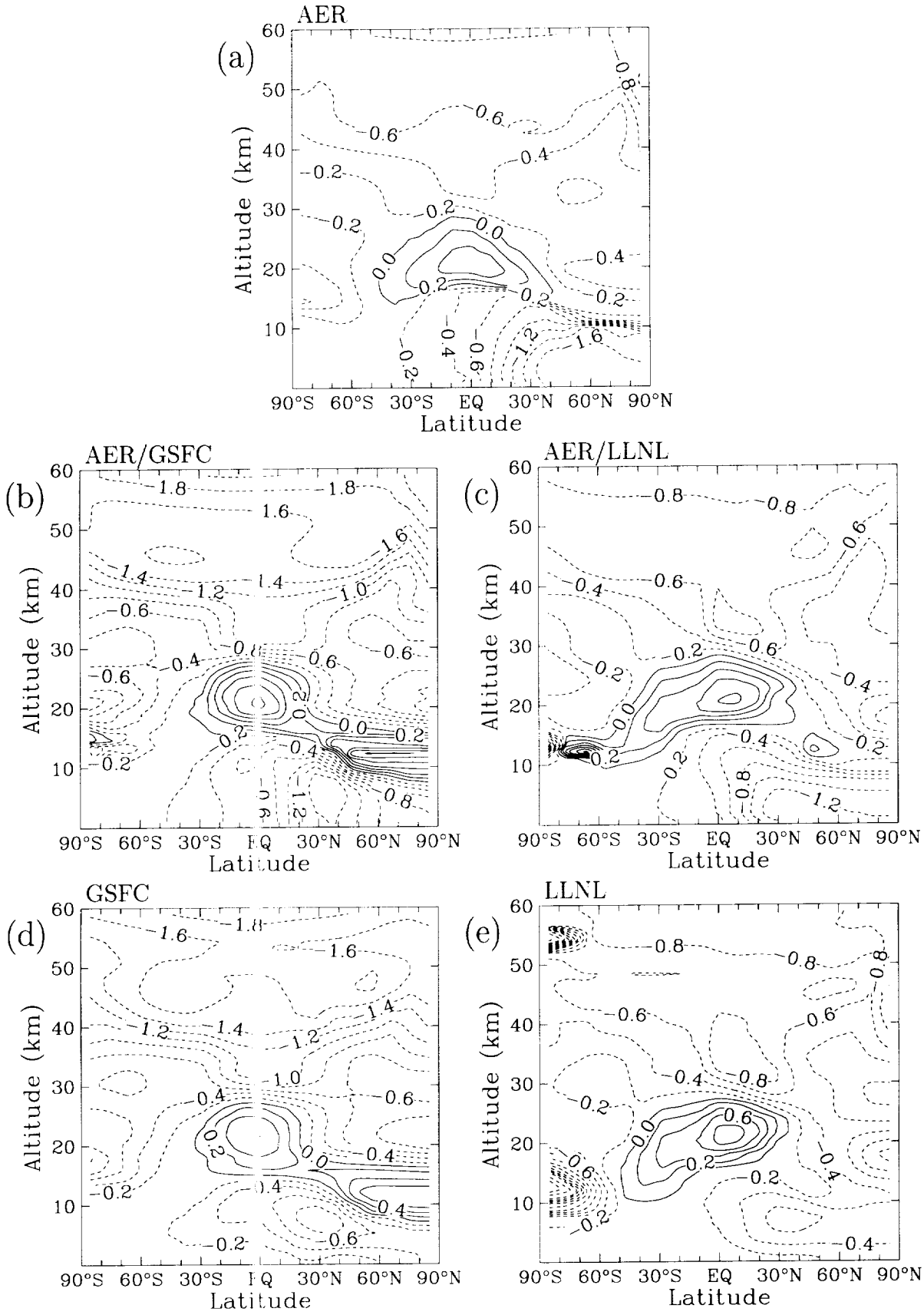

Figure 18. Calculated perturbation in O_3 (%) for October due to emission from HSCT aircraft in 2015 relative to an atmosphere with only subsonic aircraft. Panel (a) shows AER model results, panel (b) AER/GSFC results, panel (c) AER/LLNL results, panel (d) GSFC results, and panel (e) LLNL results, all without PSC chemistry.

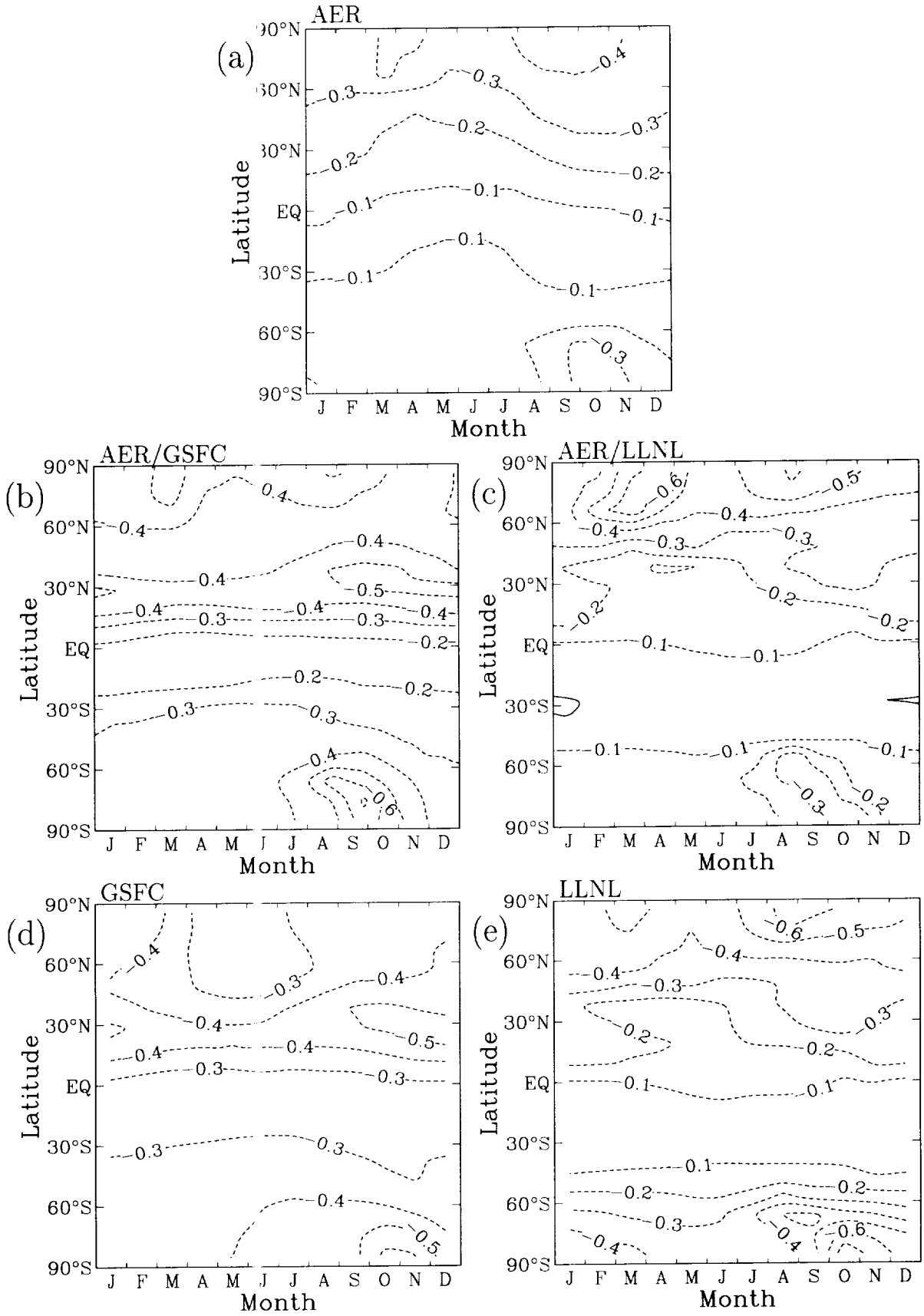

Figure 19. Calculated perturbation in O_3 column (%) due to emission from HSCT aircraft in 2015 relative to an atmosphere with only subsonic aircraft. Panel (a) shows AER model results, panel (b) AER/GSFC results, panel (c) AER/LLNL results, panel (d) GSFC results, and panel (e) LLNL results, all without PSC chemistry.

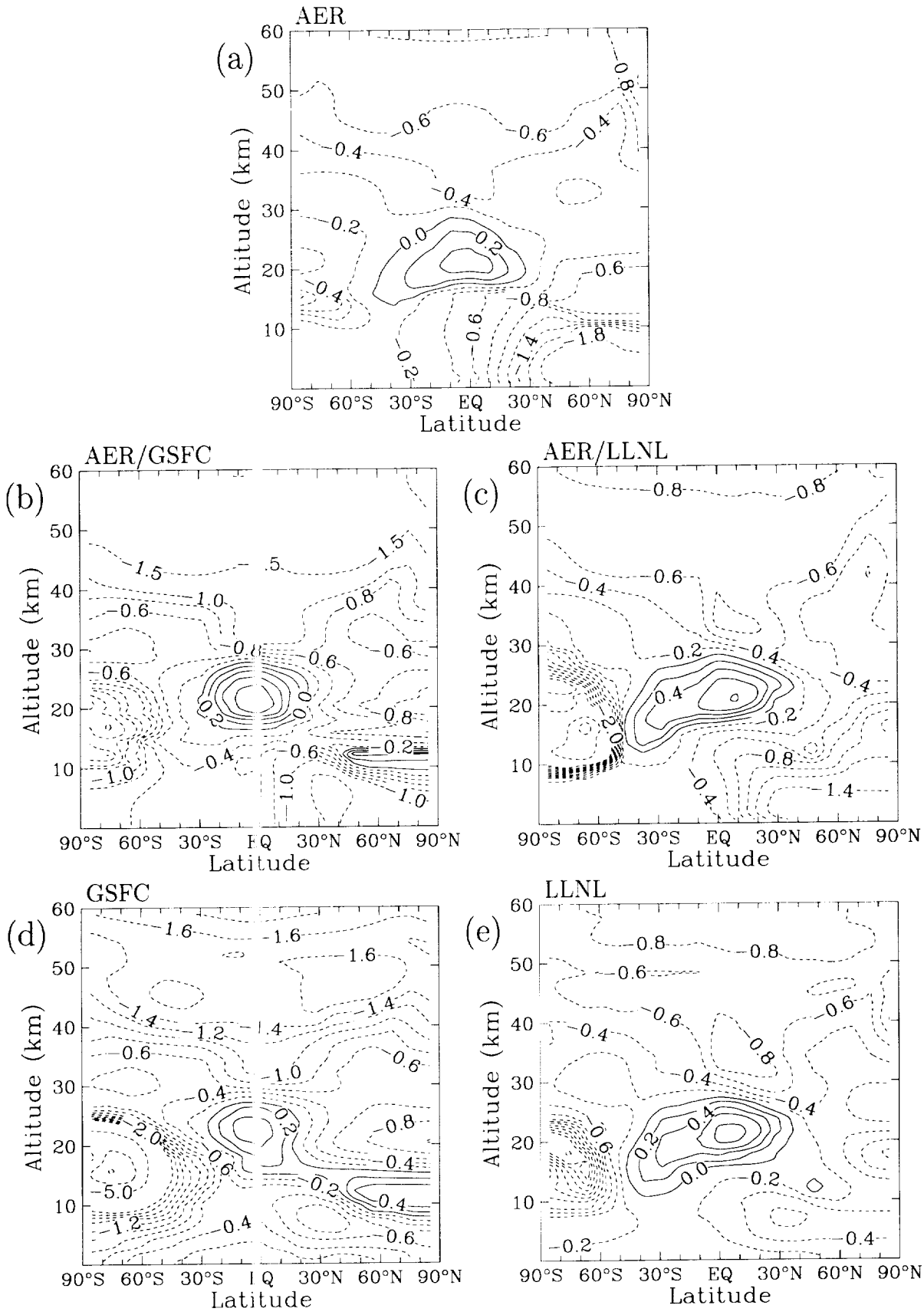

Figure 20. Calculated perturbation in O_3 (%) for October due to emission from HSCT aircraft in 2015 relative to an atmosphere with only subsonic aircraft. Panel (a) shows AER model results, panel (b) AER/GSFC results, panel (c) AER/LLNL results, panel (d) GSFC results, and panel (e) LLNL results, all with PSC chemistry.

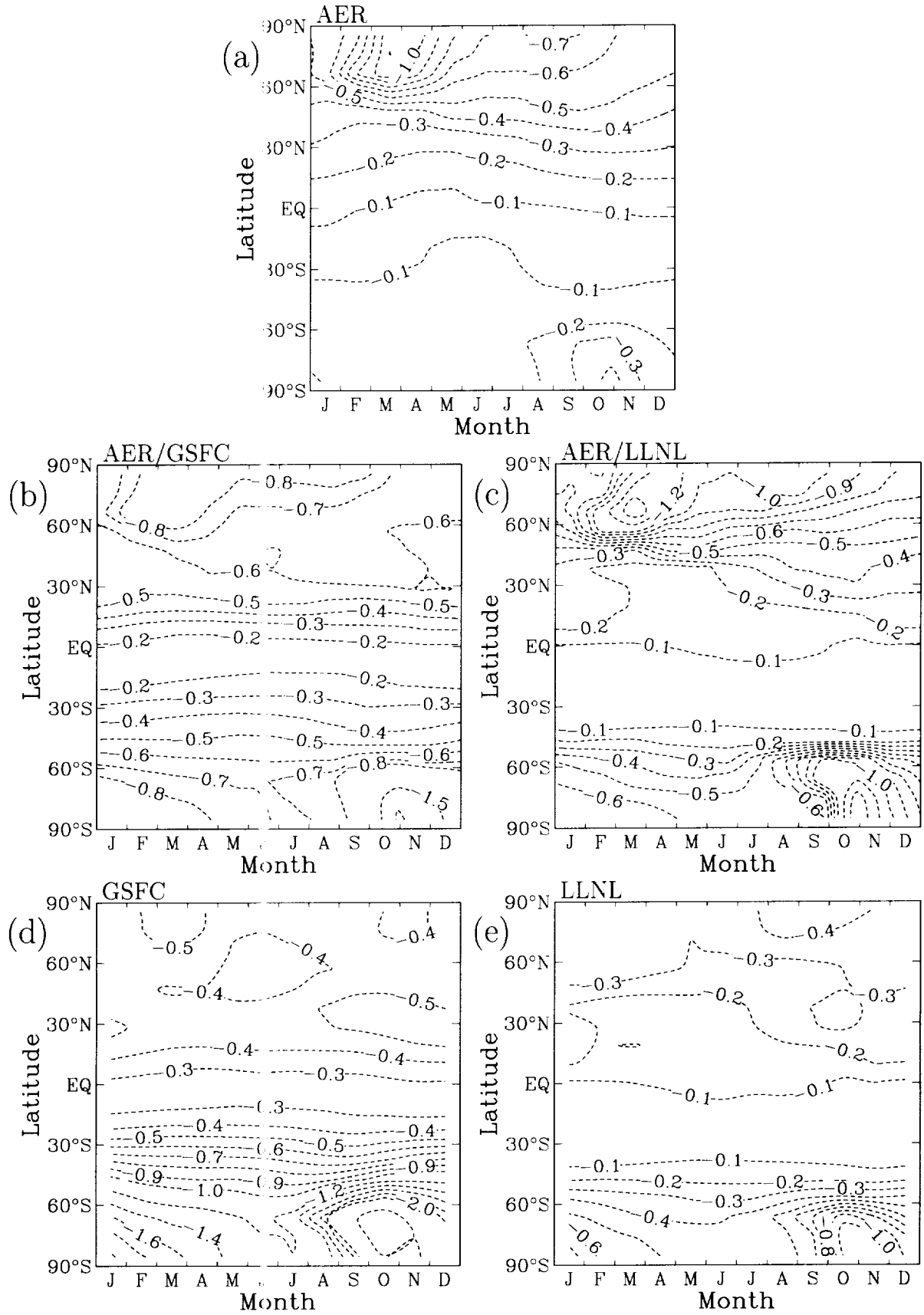

Figure 21. Calculated perturbation in O_3 column (%) due to emission from HSCT aircraft in 2015 relative to an atmosphere with only subsonic aircraft. Panel (a) shows AER model results, panel (b) AER/GSFC results, panel (c) AER/LLNL results, panel (d) GSFC results, and panel (e) LLNL results, all with PSC chemistry.